ChemPubSoc Europe

DOI: 10.1002/cphc.201201023

Unraveling the Reaction Mechanisms Governing Methanol-to-Olefins Catalysis by Theory and Experiment

Karen Hemelsoet,* Jeroen Van der Mynsbrugge, Kristof De Wispelaere, Michel Waroquier, and Veronique Van Speybroeck*[a]

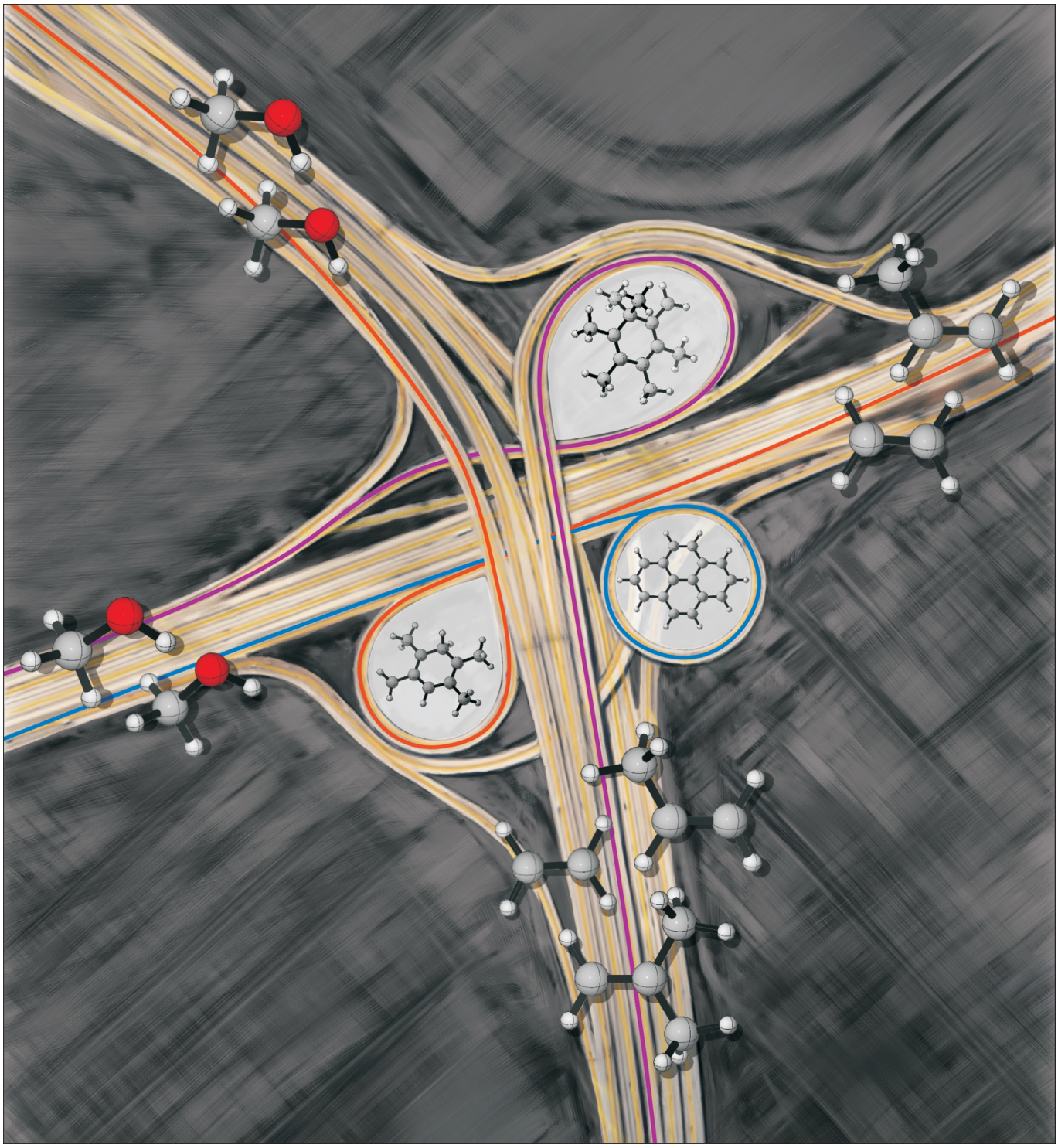

The conversion of methanol to olefins (MTO) over a heterogeneous nanoporous catalyst material is a highly complex process involving a cascade of elementary reactions. The elucidation of the reaction mechanisms leading to either the desired production of ethene and/or propene or undesired deactivation has challenged researchers for many decades. Clearly, catalyst choice, in particular topology and acidity, as well as the specific process conditions determine the overall MTO activity and selectivity; however, the subtle balances between these factors remain not fully understood. In this review, an overview of proposed reaction mechanisms for the MTO process is given, focusing on the archetypal MTO catalysts, H-ZSM-5 and H-SAPO-34. The presence of organic species, that is, the so-called hydrocarbon pool, in the inorganic framework forms the starting point for the majority of the mechanistic routes. The combination of theory and experiment enables a detailed description of reaction mechanisms and corresponding reaction intermediates. The identification of such intermediates occurs by different spectroscopic techniques, for which theory and experiment also complement each other. Depending on the catalyst topology, reaction mechanisms proposed thus far involve aromatic or aliphatic intermediates. Ab initio simulations taking into account the zeolitic environment can nowadays be used to obtain reliable reaction barriers and chemical kinetics of individual reactions. As a result, computational chemistry and by extension computational spectroscopy have matured to the level at which reliable theoretical data can be obtained, supplying information that is very hard to acquire experimentally. Special emphasis is given to theoretical developments that open new perspectives and possibilities that aid to unravel a process as complex as methanol conversion over an acidic porous material.

1. Introduction

The depletion of oil reserves and the rapidly increasing demand for base chemicals, such as ethene and propene,[1] initiated the quest for chemical processes based on alternative feedstock. In this light, methanol has gained a lot of interest because it may be transformed into gasoline (methanol to gasoline or MTG) and/or olefins (methanol to olefins or MTO) when reacted over acidic zeolite catalysts.[2–4] Methanol is an interesting alternative to crude oil, as it may be obtained from any gasifiable carbon-rich feedstock, such as natural gas, coal and biomass. A methanol-based economy, in which methanol is used as energy-storage material and fuel, as well as feedstock to synthesize hydrocarbons and their products, has been suggested by Olah.[5,6] The precise product distribution and underlying reaction mechanisms of methanol conversion vary with the choice of catalyst and process conditions. The MTG reaction was—rather accidentally—discovered by Mobil researchers when testing a newly synthesized zeolitic material H-ZSM-5 in search of new production routes towards high-octane gasoline.[7,8] For the more selective MTO process two industrial set-ups were developed in parallel, that is, the Norsk Hydro/UOP MTO process, based on the SAPO-34 catalyst and producing ethene and propene,[9] and Lurgi's process,[10] based on the ZSM-5 catalyst and predominantly producing propene with some gasoline as byproduct.

Mechanistic investigations began almost immediately after the discovery of the MTG and MTO processes. Haw and coworkers summarized the different stages which occur during the overall conversion process.[11] Some of these stages are schematically depicted in Figure 1. During the first stage, an equilibration is reached among methanol, dimethyl ether, and water. The first hydrocarbon products are formed after a kinetic induction period. In a later stage, secondary reactions convert the primary products into a mixture of other hydrocarbons. Finally, coke species are formed and the catalyst is deactivated. The overall mechanistic process is very complex as a lot of reactions occur both in a consecutive and/or competing fashion. This review focuses on the mechanistic routes underlying the formation of light olefins on the one hand and the formation of coke species on the other hand. The production of light olefins is the main aim of the MTO process, and the underlying reaction mechanisms are called the active routes. In contrast, the formation of coke is highly undesirable, and the underlying routes are called the passive routes.

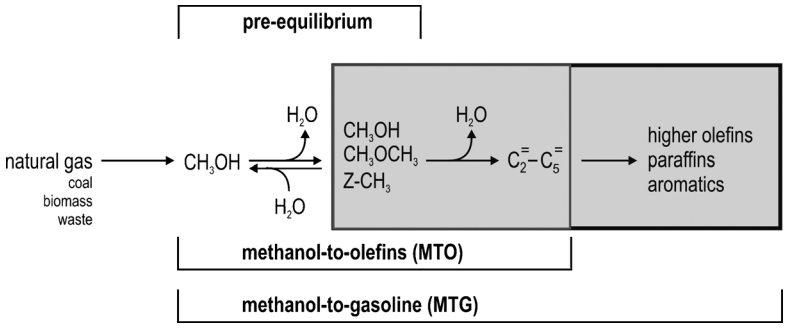

Figure 1. Conversion of natural gas into methanol and subsequent reactions.

[a] *Prof. Dr. K. Hemelsoet, J. Van der Mynsbrugge, K. De Wispelaere, Prof. Dr. M. Waroquier, Prof. Dr. V. Van Speybroeck*
Center for Molecular Modeling (CMM), Ghent University
Technologiepark 903, B-9052 Zwijnaarde (Belgium)
and
QCMM-alliance, Ghent-Brussels (Belgium)
E-mail: karen.hemelsoet@ugent.be
veronique.vanspeybroeck@ugent.be

Various experimental techniques have been employed to study MTO conversion and have provided important clues regarding the reaction mechanisms. Isotopic labeling experiments, using ^{13}C-labeled methanol[12–15] or to a minor extent H/D exchange[16–19] have been used extensively. The contents of the zeolite pores may be examined by either destructive or non-destructive methods. Using the former approach, the process is halted by quenching and the catalyst is subsequently digested in hydrofluoric acid to release the trapped species, which are then examined using gas chromatography–mass spectroscopy (GC-MS).[20] Alternatively, in situ NMR spectroscopy[21] or vibrational (FT-IR or Raman) spectroscopy can be used to track intermediates in real time. UV/Vis spectroscopy also provides additional insight when larger (poly)aromatic species are involved, which is typically the case for the coke molecules[22] (see Section 5). Spatiotemporal spectroscopy nowadays allows characterizing catalysts at work; Buurmans and Weckhuysen reviewed this booming field and highlighted the truly heterogeneous and dynamic structure of real catalyst materials.[23] Most studies investigating the MTO mechanism involve the ZSM-5, SAPO-34, and Beta catalysts. Beta zeolite is mostly used as a model catalyst for understanding the activity and selectivity of reaction intermediates. The combination of theory and experiment enables a detailed description of reaction mechanisms and corresponding reaction intermediates. Theo-

Karen Hemelsoet is an assistant professor at the Ghent University within the faculty of engineering and architecture (Belgium) and leads the computational spectroscopy division within the Center for Molecular Modeling. She graduated as an engineer in physics in 2002 and obtained her PhD in 2007. During her PhD she studied reactivity indicators and coke species using first-principle simulations. After her PhD she received a postdoctoral fellowship from the National Fund for Scientific Research Flanders. She stayed one year in the group of inorganic chemistry and catalysis of Utrecht University (The Netherlands) of Prof. B. Weckhuysen, focusing on computational absorbance spectroscopy involving zeolites. Present research interest is mainly computational spectroscopy for studying various systems, such as flexible dyes and catalytic materials.

Jeroen Van der Mynsbrugge studied chemical engineering at the Ghent University. He received his Master's degree in 2009 for his thesis studying the alkene route for MTO conversion in H-ZSM-5 using molecular modeling. He is currently pursuing a PhD degree under the supervision of Professor Van Speybroeck at the Center for Molecular Modeling. His research interests include adsorption and catalysis in zeolite materials.

Kristof De Wispelaere is currently a PhD fellow at the Center for Molecular Modeling. Before, he obtained his MS degree in chemical engineering at Ghent University and did his master thesis at the Center for Molecular Modeling on the deactivation of zeolite and zeotype catalysts in the MTO process. After graduation he received a predoctoral fellowship from the Research Foundation Flanders (FWO). His current research projects focus on the theoretical modeling of olefin production during the MTO process in zeotype materials.

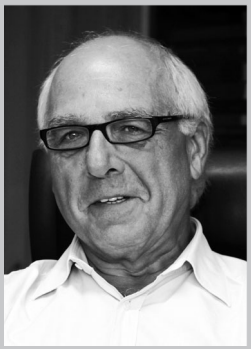

Michel Waroquier is full professor in physics at the Ghent University. In 1997 he founded the Center for Molecular Modeling (CMM) together with Professor Veronique Van Speybroeck. He succeeded in building his team up to more than 30 people, mainly physicists and chemists. The current research areas cover biochemistry (structure and function determination), organic chemistry (chemical kinetics, solvent effects), spectroscopy (EPR, NMR, IR, Raman), computational materials research on the nanoscale, and nanoporous materials (synthesis, chemical kinetics). His main interest goes to model development and validation of the new models in computational applications.

Veronique Van Speybroeck is full professor at the Ghent University within the faculty of engineering and architecture. She graduated as engineer in physics at the Ghent University in 1997 and obtained her PhD in 2001. She was co-founder in 1997 of the Center for Molecular Modeling (CMM, http://molmod.ugent.be) which is currently composed of about 35 researchers. In this center, she is leading the computational molecular modeling division. After her PhD she received a postdoctoral fellowship from the National Fund for Scientific Research Flanders. Since 2007, she holds a position as Research Professor. Her current research interests primarily comprise study of the kinetics of chemical reactions with state of the art molecular modeling techniques. In 2010, she received an European Research Council (ERC) starting grant on a subject dealing with accurate prediction of chemical kinetics of catalytic reactions taking place in nanoporous materials from first principles.

retical simulations offer the advantage that they enable isolating individual elementary steps and separating the influence of distinct properties such as catalyst topology and chemical composition. More recently, ab initio simulations allowed the determination of reliable kinetic data for individual reaction steps with inclusion of the zeolite environment, which is required to discriminate between different catalytic cycles.[24,25] Obtaining this information experimentally is very difficult, as many reactions are taking place simultaneously and theory can serve as a valuable complementary tool to unravel the mechanism.

In zeolite catalysis, shape selectivity is a crucial issue. Shape selectivity can manifest itself in different forms, in particular reactant, transition state, and product selectivity, as depicted in Figure 2 for a fictitious zeolite structure. The catalyst topology

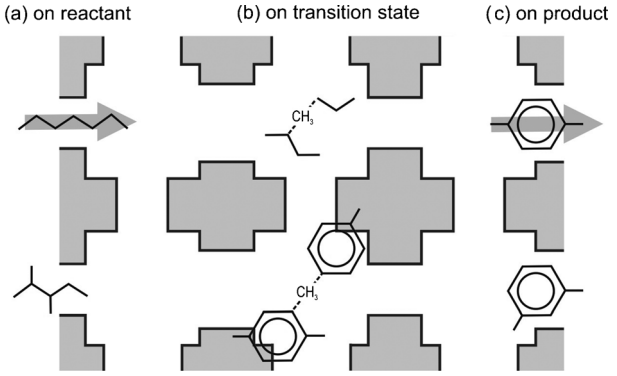

Figure 2. Fictitious zeolite structure illustrating different manifestations of shape selectivity (ref. [26]).

largely determines the type of shape selectivity that will be dominant for a certain reaction. One can distinguish between large-, medium-, and small-pore zeolites, exhibiting 12-, 10- or 8-ring pore windows, respectively. In case of the MTO reaction, reactant-shape selectivity is not considered crucial due to the small size of methanol (free diameter of 2.8 Å, compared to window openings of 7, 5.5, and 4 Å for large-, medium-, and small-pore zeolites). The importance of transition state or product-shape selectivity depends on the specific topology and detailed process parameters,[2] and is discussed in Sections 4 and 5 for the active and passive routes.

H-ZSM-5 and H-SAPO-34 are known as the archetypal MTO catalyst materials and are already used for commercial methanol conversion. Their topological differences, as well as differences in chemical composition, lead to distinct product selectivity and coking behavior. These materials have been studied in detail from both an experimental and theoretical viewpoint. H-ZSM-5 has the MFI topology, exhibiting a 3D network consisting of sinusoidal (5.1×5.5 Å^2) and straight (5.3×5.6 Å^2) channels defined by 10-rings resulting in medium-sized pores.[27] H-SAPO-34 is a small-pore material, featuring the CHA topology, in which spacious cavities (10.0×6.7 Å^2) are connected by small (3.8×3.8 Å^2) 8-ring windows.[27] In addition to H-ZSM-5 and H-SAPO-34, H-Beta (BEA) has also been employed for mechanistic investigations since it consists of a network of intersecting (straight) channels which are slightly larger compared to H-ZSM-5. Its more spacious channels minimize steric constraints and transition-state selectivity, and enable direct feeding of bulky intermediates to the catalyst. In recent years, other zeolite materials have also been tested for their use as MTO catalysts. The search for an optimal catalyst for the conversion of methanol is ongoing, as is further discussed in Sections 4 and 6. A selection of materials which have either been tested or which are promising for MTO conversion is given in Figure 3, along with the indication of topological details.[27] In addition to the MFI, CHA and BEA topology, the AFI and TON—exhibiting a 1D channel system—and the DDR topology are shown.

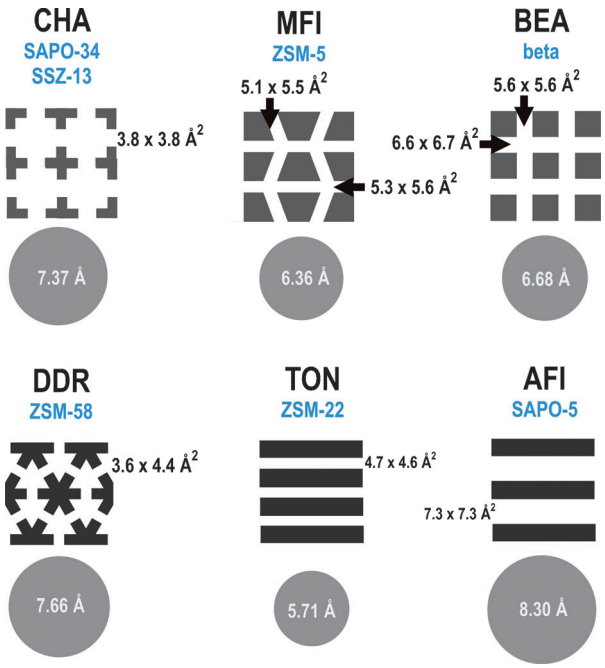

Figure 3. Representation of various MTO catalyst materials, with indication of relevant pore sizes and pore openings. In grey, the maximum diameter of a sphere which can be included is also given. The numbers refer to pure silica zeolites and are taken from the IZA database.[27]

Besides the topology, the MTO activity and selectivity also crucially depend on the acid strength of the catalyst material. The acid character mainly results from Brønsted acid hydroxy groups, and their presence can be measured using IR spectroscopy.[28–31] The number, distribution, and strength of acid sites depend on the synthesis conditions of the catalyst involved, and have proven challenging to control. Some theoretical aspects related to this topic are discussed in Section 2.1, as they benefit from recent advances in computational chemistry. Dai and co-workers recently showed that the MTO reaction can occur over low-silica aluminophosphates, indicating that only a minimal Brønsted acid site density is required.[32]

Recently, a comprehensive review by Olsbye and co-workers was published, focusing on how zeolite cavity and pore size control product selectivity in the methanol-to-hydrocarbons (MTH) process. Particular emphasis was given to the commer-

cial aspects of methanol conversion.[2] In the current contribution we focus on the mechanistic aspects of the MTO reaction, and particularly on the insights gained from computational chemistry into this complex industrial process. Catalytic and spectroscopic techniques investigating the MTO reaction mechanisms are also addressed and their main conclusions are highlighted. Finally, we present some remarkable developments which have emerged due to recent advances in computational chemistry and/or experimental set-ups, providing an outlook on future MTO research.

2. Advances in Molecular Modeling in Heterogeneous Catalysis

The structure-activity relation of zeolites or zeotype materials remains often puzzling. State-of-the-art theoretical simulations are an ideal approach to explore these complex materials. Most studies have been focusing on the simulation of accurate energetic data and reaction barriers.[25] The calculation of rate coefficients of individual reaction steps in heterogeneous catalysis has only recently become possible.[24] Modeling the Brønsted acid sites is a key aspect, and is discussed in Section 2.1. Subsequently, Section 2.2 reviews the different models to account for the nanoporous environment of these active sites.

2.1. Modeling the Brønsted Acid Sites

In MTO, Brønsted acid sites originating from framework substitutions (Al or Si) and their charge-compensating protons are mainly responsible for the catalytic activity. Numerous studies, primarily on H-ZSM-5 and H-SAPO-34, have focused on the position of these acid sites and their distribution throughout the material. An interesting approach for studying the acidity of zeolitic materials is the combination of experimental IRMS-TPD of ammonia and density functional theory (DFT) calculations[33–36] which allows for the identification of Brønsted acid OH sites, as has been shown for H-SSZ-13[33] and H-SAPO-34.[37]

Attempts to determine the energetically most favorable position for aluminum substitution in H-ZSM-5 have ultimately found little preference for any specific T-site.[38–42] Moreover, recent experimental and theoretical evidence indicates that the distribution of framework aluminum throughout the zeolite material is kinetically controlled during its synthesis.[43–45] In several theoretical studies, Al is inserted at the T12 position, which is located at the intersection of the straight and sinusoidal channels of the MFI structure, and hence offers maximal available space to accommodate various guest molecules.[42,46] For a given aluminum substitution, the compensating proton may still be located on any of the four neighboring framework oxygens. However, protons can migrate from one oxygen bridge to another, which is facilitated when assisted by adsorbate species, such as for example, water molecules.[47–51]

As for H-ZSM-5, DFT simulations on CHA-type zeolites indicated that energetic differences between various proton locations are below 10 kJ mol^{-1}; computed values depend on the chosen model of catalyst material and level of theory.[52] Several studies on H-SAPO-34 have investigated the distribution of silicon framework atoms and the location of framework hydroxyl groups.[53] Silicon insertion in aluminophosphates (AlPOs) can occur either by substitution of a single P atom by Si and a proton, or by substitution of two neighboring Al and P atoms by two Si atoms, or by a combination of both, depending on the template choice, synthesis conditions, and so forth.[53–56] The combined mechanism leads to the formation of silicate islands, which have been shown to possess strong acid sites at their borders.[57,58] Barthomeuf argued on topological grounds that silicate aggregates will always be present for Si fractions above 11 %;[59] and this has been observed using magic angle spinning nuclear magnetic resonance (MAS NMR) spectroscopy.[53,60] The stability of the aggregates has been confirmed using theoretical simulations by Sastre et al.[58,61] To date, theoretical studies on MTO using H-SAPO-34 have only considered isolated acid sites.[62,63]

2.2. Modeling the Nanoporous Environment

Initial theoretical studies investigating the MTO reaction mechanism were based on simple gas-phase computations, in which small zeolite clusters consisting of three to five T-atoms mimic the bridging Brønsted site.[64–73] In these calculations, the catalyst's specific framework structure is completely disregarded, such that acquired results do not explain the influence of topology. Increasing computational resources combined with more efficient software implementations have enabled a more complete description of the catalyst structure. In contemporary studies, two approaches are followed to represent the nanoporous environment, that is, the use of extended finite clusters and the use of periodically repeated unit cells. Both model types are depicted in Figure 4 for a catalyst with CHA topology.

Simulations applying periodic boundary conditions on a complete unit cell (Figure 4a), which is then infinitely repeated, are in principle most suitable to capture the true nature of a nanoporous material. However, supercells are sometimes necessary to prevent unphysical interactions between bulky reactants; this is for example, the case for a CHA topology due to its small unit cell. On the other hand, an accurate description of the local environment surrounding the active site is equally crucial to obtain reliable results on investigated reactions. As such, extended clusters offer more flexibility, since a wider variety of computational methods, such as most recent functionals, may be employed. In addition, methods to localize transition states are well established for cluster calculations. In the extended-cluster approach (Figure 4b), the catalyst is modeled by a zeolite fragment large enough to capture the topological effects necessary to adequately describe the active site. Terminating hydrogen atoms are fixed in space to prevent the unphysical collapse of the cluster during geometry optimization. ONIOM (our own *N*-layered integrated molecular orbital and molecular mechanics) schemes combining quantum mechanical methods and classical molecular mechanics (QM/MM) or different quantum mechanical methods (QM/QM) are often used to reduce the computational expense of treating a large molecular system. Thermochemical data, such as adsorption

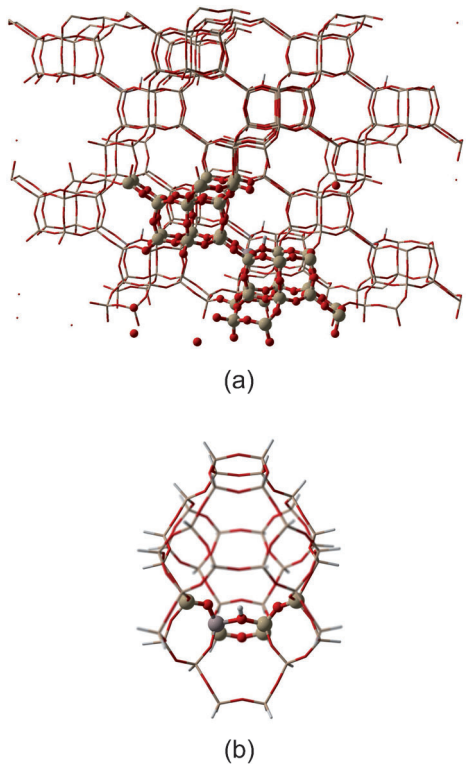

Figure 4. Representation of a unit cell (indicated with balls and sticks), 2×2×2 periodically repeated (a) and a finite extended cluster (with indication of a ONIOM high-level with balls and sticks) (b) of a proton-exchanged zeolite with CHA topology.

enthalpies as well as rate coefficients of reactions, are calculated based on molecular partition functions. In most programs this is achieved by performing a normal mode analysis (NMA), that is, diagonalizing the (mass-weighted) Hessian matrix containing the second derivatives of the energy with respect to the atom positions. The resulting eigenvalues and eigenvectors are the frequencies and vibrational modes respectively. This approach neglects all anharmonic motions which might be important in some cases, however, methods to go beyond the harmonic oscillator (HO) approximation are not straightforwardly applied for zeolite models systems.[24] As the NMA is computationally very demanding, several schemes have been developed to deal with extended systems. Partial Hessian vibrational analysis (PHVA) limit the computational cost by considering some atoms to be fixed in space. The rows and columns corresponding to the fixed atoms are consequently deleted from the Hessian and then this smaller submatrix is diagonalized. When only part of the geometry is optimized such PHVA method is mandatory to prevent negative spurious frequencies.[74–76] The PHVA model has successfully been applied in MFI- and CHA-type catalysts, leading to thermodynamic and kinetic data for relevant individual reaction steps.[24,62,77–80] Furthermore, the mobile block Hessian (MBH) method has been developed, in which groups of atoms are considered as blocks during vibrational analysis.[74,75] Individual atom motions are not allowed in the block, but the block as a whole can translate and rotate as a rigid unit. A combined PHVA-MBH scheme has been used to analyze IR spectra of small alcohols (methanol and ethanol) and hydrocarbon pool (HP) compounds in an extended H-SAPO-34 cluster.[81] Using this theoretical approach, the SAPO skeleton motions could be filtered out and IR peak shifts due to framework-guest interactions could be identified. In the case of the aromatic hydrocarbons, an average peak shift (comparing IR spectra of gas-phase compounds with those of the supramolecular complex) of 12 and 44 cm^{-1} is reported for the ν(C=C) and ν(CH) vibrations.[81]

In both extended-cluster and periodic studies, mostly DFT methods are nowadays applied since they offer reliable data at a reasonable cost. Notably, the implementation of van der Waals interactions in the framework of DFT was a crucial step forward.[82,83] These interactions are very important as adsorption enthalpies calculated with and without dispersive corrections can differ substantially, ranging from 30 to 70 kJ mol^{-1} (for methanol and butene in H-ZSM-5),[25,84] whereas intrinsic reaction barriers (for methylations at alkenes in H-ZSM-5) may differ by 10–20 kJ mol^{-1}.[24,25] One of the most effective and most widely applied methods to account for dispersion is the so-called DFT-D scheme proposed by Grimme.[85–87] In this method, an empirical damped-potential term, that is, $-C_6R^{-6}$, is added to the energies obtained with standard functionals, at no extra computational expense. Another possibility is the use of DFT functionals which have been especially parameterized to describe non-covalent interactions; examples are M06-2X[88] and ωB97XD.[89]

The performance of cluster calculations versus periodic calculations has been a topic of debate. Each method has its strengths and weaknesses. This issue has been discussed by Nguyen et al. using the adsorption of C_1–C_4 alcohols in H-ZSM-5 as a case study.[90] Of direct importance for the MTO process is the detailed study of methylation reactions on alkenes in H-ZSM-5 for which experimental kinetic data are available.[12,13] Svelle et al. have shown that enthalpy barriers can be calculated with near chemical accuracy by combining MP2 energy calculations with periodic DFT calculations (see Figure 5).[25] This hybrid approach is computationally very demanding and cannot routinely be applied. A more feasible procedure is

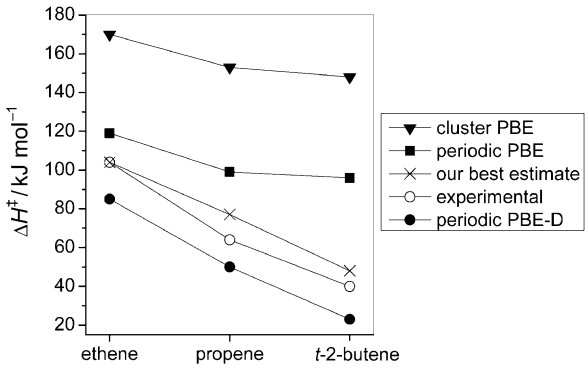

Figure 5. Apparent enthalpy barriers for the methylation of alkenes in H-ZSM-5 obtained with various computational schemes as compared to experimental data. Results indicated by (×) correspond to the hybrid MP2:DFT-based scheme. (Reprinted with permission from ref. [25]. Copyright 2009 American Chemical Society.)

based on large finite clusters using cost-efficient hybrid DFT functionals, predicting also accurate enthalpy barriers. As an additional advantage, this method allows for the computing of rate coefficients (hence including entropic contributions). Simulated relative methylation rates for ethene, propene, and butene in H-ZSM-5 ($k_{ethene}/k_{propene}/k_{butene}$ = 1:23:763) reproduce the experimental data very well ($k_{ethene}/k_{propene}/k_{butene}$ = 1:17:50) as depicted in Figure 6.[24]

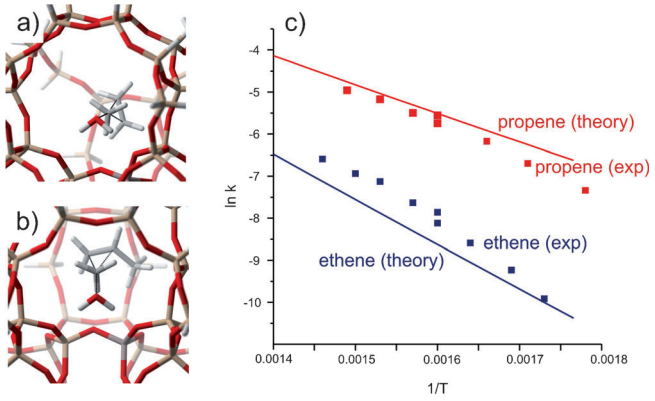

Figure 6. Transition state geometries for ethene (a) and propene (b) methylation in H-ZSM-5, and corresponding Arrhenius plots—*k* expressed in mol g_{cat}^{-1} h^{-1} $mbar^{-1}$ and *T* in K—(c) comparing theoretical and experimental results. (Adapted and reprinted from ref. [24]. Copyright 2011 American Chemical Society.)

So far, most theoretical studies have applied models that represent idealized catalytic materials, limiting the attainable agreement between experiment and theory. Real catalyst materials are known to be truly heterogeneous, in both a space- and time-like manner[91] and a fully periodic structure does not capture this heterogeneity. Modeling of this heterogeneity and modeling of framework defects, such as mesopores, terminal silanol groups and extra-framework species (see Section 6) remain challenges for future research.

3. Reaction Mechanisms: Hydrocarbon Pool Consensus

The mechanism governing the MTO process has been one of the most controversial in heterogeneous catalysis. Initially, olefin formation was thought to occur through a direct mechanism, in which C–C bonds are formed from the direct coupling of C_1-species derived from methanol or dimethyl ether. Several direct mechanisms were proposed, featuring intermediates such as oxonium ylides, carbenes, carbocations, free radicals, or surface-bound alkoxy species.[92] None of these were successful in explaining all experimental observations. In several experiments, a delay had been observed between the start of the process and the first olefin products showing up in the reactor effluent.[93–95] Methanol conversion is very low at the start of the process, but rises steadily to 100% after some time on stream. The occurrence of this so-called kinetic induction period is particularly difficult to reconcile with any direct mechanism.[96] Theoretical calculations have been employed in an attempt to corroborate the many mechanistic proposals. As a result, scattered evidence in favor of direct mechanisms may be found in the literature, but most of these studies only show the feasibility of a few key steps, and no complete pathway starting from methanol and leading to olefin production could be proposed. Lesthaeghe et al. performed a rigorous DFT-based theoretical study on a large number of previously suggested direct mechanisms combined in a single scheme.[97] The authors were able to show that every imaginable pathway features at least one unstable intermediate or highly activated reaction step and no uninterrupted route to ethene or propene formation can therefore be identified.[97,98]

An alternative indirect mechanism was first proposed by Dessau and co-workers.[99,100] In their view, the actual product formation only takes off after a critical amount of alkenes has been formed during the induction period. Once steady-state methanol conversion is attained, ethene and higher alkenes are mainly produced from repeated methylation, oligomerization, and cracking reactions. Around the same time, Mole et al. reported a greatly enhanced rate of methanol conversion when small amounts of aromatics such as toluene and *p*-xylene are added to the MTH reaction.[101,102] Similar ideas were advanced independently by Langner from co-feeding cyclohexanol with methanol.[103]

These studies inspired Dahl and Kolboe when they formulated their indirect mechanism proposal in the early 1990s (Figure 7).[104–106] Dahl and Kolboe suggested that a pool of hydrocarbons present in the zeolite pores acts as a co-catalyst for the MTO conversion. These HP species grow through repeated methylation and subsequently eliminate light olefins, regenerating the HP molecule and closing the catalytic cycle.[104,105] The crucial role of the interplay between the HP species and the zeolite framework led Haw et al. to the concept of a supramolecular catalyst for the MTO process,[96] with unique properties determined by both the zeolite characteristics (composition, topology, acid strength) and the nature of the species present in the pores. This concept of a supramolecular catalyst is schematically depicted in Figure 8.[11,96]

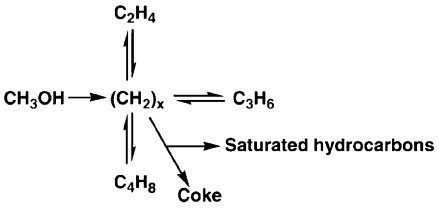

Figure 7. Indirect hydrocarbon pool reaction mechanism. (Reprinted with permission from ref. [104]. Copyright 1993 Springer.)

The exact nature of the HP species was initially unspecified. However, in their own experiments on H-SAPO-34, Dahl and Kolboe had observed that co-feeding ethene or propene has little effect on methanol conversion and these alkenes remain mostly inert, in contrast to the co-reaction with benzene deriv-

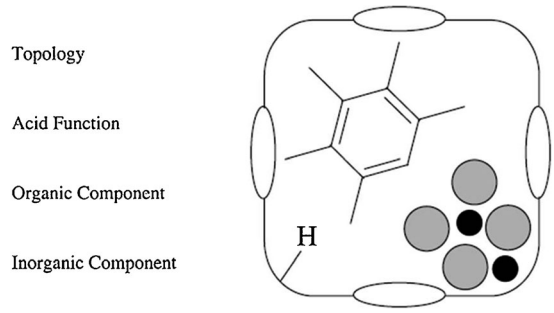

Figure 8. View of a single cage in a supramolecule zeolite catalyst for MTO conversion, with indication of its four key features as proposed by Haw et al.[96] (Reprinted with permission from ref. [96]. Copyright 2005 Springer.)

atives.[104,105] Combined with earlier reports from Mole et al.,[101,102] these observations prompted further investigation of the hypothesis that aromatic species are the key components in the HP by Arstad and Kolboe[68,69] and by Haw and coworkers.[11,96,107–110] The importance of cyclic carbenium ions and heavily methylated benzenes as organic reaction centers inside the pores of an MTO catalyst was established for both H-SAPO-34 and H-beta.[96,111–113] Figure 9 displays important HP species in H-SAPO-34 and H-ZSM-5. In addition to lower-methylated benzenic compounds, methylated cyclopentenyl cations have been observed by NMR spectroscopy during MTO conversion on H-ZSM-5 and hence these species were also suggested as potential reaction centers in H-ZSM-5.[114] The protonated forms of the HP species are generally accepted as the most important intermediates during methanol conversion.

Gas-phase proton affinities (PAs) have been used to assess the stability of these carbocations; an overview of reported values for methylated (poly)aromatics can be found in Table 1. Polymethylbenzenes (PMBs) with a PA value higher than 820 kJ mol^{-1} have been shown to occur mostly in their protonated form inside H-Beta.[115,116] In addition, Macht et al. pointed out the subtle balance between the acid strength of the catalyst (as indicated by its deprotonation energy), the proton affinity of the reactants, the interaction energy between cations and anions at the transition state, and reactant-adsorption energy.[117]

Some recent studies report alternative intermediates. By means of IR spectroscopy and GC-MS experiments with deuterated or ^{13}C-labeled methoxy groups, Yamazaki et al. observed carbene-like intermediates during the reaction of methoxy groups and ethene in H-ZSM-5, mordenite, H-SSZ-13, and HY.[19] Their results are in line with an earlier study by Hunger et al.[122] Characterization of the HP compounds is still ongoing, and accompanies the search for reaction routes discussed in Sections 4 and 5.

The origin of the HP also remains a puzzling question. Initially, direct C–C coupling, while inefficient and therefore insignificant during the steady state phase of the MTO process, was thought to play a role during the induction period. Experiments performed by Song et al.[123] using highly purified reagents, carrier gases, and catalysts, however, have shown that methanol is almost completely unreactive under these conditions, suggesting that direct C–C coupling might effectively never take place and the HP grows from reactions with carbonaceous impurities present in regular methanol feeds and/or zeolite crystals. This is opposed to observations made by Jiang et al., stating that traces of organic impurities present in the methanol do not influence the formation of primary hydrocarbons from surface methoxy groups.[124] Although not experimentally confirmed, a theoretically plausible route has been proposed for the ship-in-a-bottle formation of cyclic HP compounds inside the H-ZSM-5 framework, starting from small hydrocarbon fragments and methanol.[80]

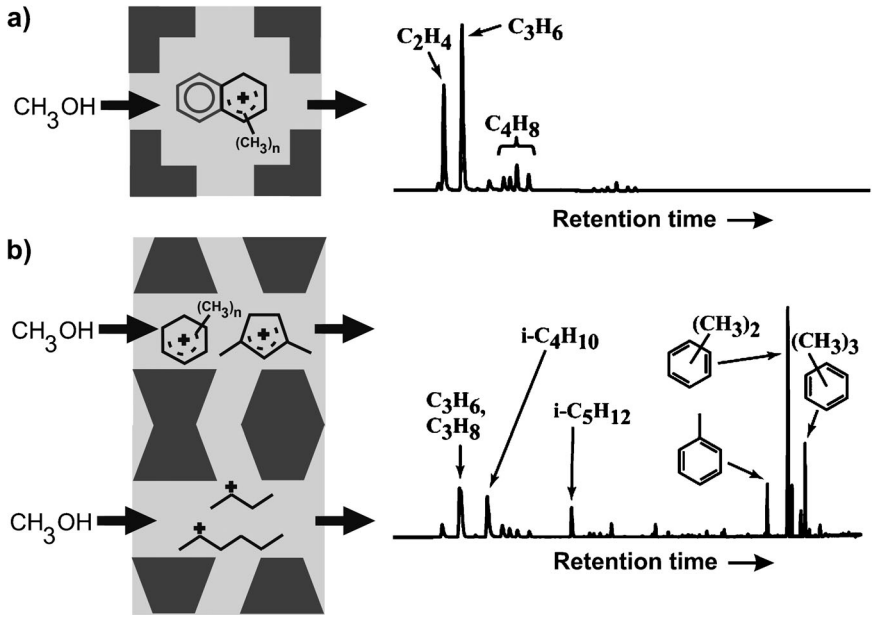

Figure 9. Representation of the main HP species in H-SAPO-34 (a) and H-ZSM-5 (b). *n* refers to the number of methyl substituents on the aromatic rings. Corresponding chromatograms illustrate the product selectivity for both materials under identical conditions (taken from ref. [113]; experiments using 300 mg of catalyst operated at 723 K, products sampled 1.5 s following pulse introduction of 10.2 μL of methanol). (Reprinted with permission from ref. [113]. Copyright 2003 American Chemical Society.)

4. Reaction Mechanisms for Alkene Production: Active Routes

With the HP hypothesis as a starting point, the challenge of identifying actual catalytic cycles leading to olefin formation from methanol remains. The observation that differences

Table 1. Calculated (G3MP2[a] and B3LYP/DGTZVP[b]) and experimental (NIST database) proton affinities for different aromatic HP compounds in kJ mol^{-1}.

	position	G3MP2[118]	B3LYP/DGTZVP[119,120]	experiment[121]
benzene		744	763	750
toluene	1		758	
toluene	4	779		784
o-xylene	1		796	
o-xylene	4	790		794
m-xylene	4	805		812
p-xylene	2	787		796
1,2,3-triMB	4	814		
1,2,4-triMB	4		813	
1,2,4-triMB	5	816		
1,3,5-triMB	2	828		836
1,2,3,4-tetraMB	5	825		
1,2,3,5-tetraMB	4	837		846
1,2,4,5-tetraMB	1		838	
1,2,4,5-tetraMB	3	818		
pentaMB	3		860	
pentaMB	6	846		851
hexaMB		860	880	861
naphthalene	1		821	
1-MN	1		814	
1,2-dMN	2		828	
1,4,5-triMN	4		869	
1,4,5,6-tetraMN	1		887	
1,2,5,7-tetraMN	1		870	
1,2,4,5,8-pentaMN	2		859	
1,2,3,4,5-pentaMN	5		888	
phenanthrene	1		836	
1-MPh, pos	1		830	
9-MPh, pos	9		828	

[a] Calculated at 298 K. [b] Calculated at 0 K.

in both topology and chemical composition of the catalyst lead to totally different product streams complicates the issue even further and raises an important question with respect to product selectivity. As an example, the GC-MS total ion chromatograms of the effluent obtained after MTO conversion on H-SAPO-34 and H-ZSM-5 under identical conditions, reported by Haw and co-workers, are displayed in Figure 9.[113] While fairly bulky molecules can fit the cages of H-SAPO-34, these cannot migrate through the 8-ring windows connecting these cages (see topological details in Figure 3). Consequently, the product stream consists of small hydrocarbons, predominantly ethene and propene (see Figure 9a). On the other hand, the 10-ring channels in H-ZSM-5 are wide enough for methyl benzenes with up to four methyl groups (e.g. durene) to diffuse out of the catalyst (see Figure 9b). Besides methylbenzenes and light alkanes, especially isobutane and isopentane are formed, but only small quantities of olefins. Notably, the product composition over H-ZSM-5 depends strongly on the operating conditions. Section 4.1 reviews the mechanisms involving aromatic HP intermediates that have been proposed thus far. Since these mechanisms were not able to explain all observations (especially for H-ZSM-5), a new type of route involving aliphatic intermediates (Figure 9b) has been proposed, discussed in Section 4.2. These sections deal with H-SAPO-34, H-ZSM-5, and H-beta; the use of other zeolite materials for MTO is reviewed in Section 4.3.

4.1. Aromatic-Based Cycles: Side-Chain versus Paring

Figure 10 displays the two types of reaction cycles that have been proposed thus far for olefin formation through aromatic intermediates: the paring and the side-chain methylation mechanisms. Paring-type reactions were first proposed by Sullivan et al. in 1961[125] and should be seen as subsequent ring-contraction and -expansion reactions. The side-chain mechanism, introduced by Mole and co-workers in 1983[101,102] and further elaborated by Haw and co-workers[111,126] explains olefin formation by deprotonation to form an exocyclic bond, followed by successive side-chain methylations and subsequent side-chain elimination. Both mechanisms start with repeated methylations until a gem-methylated species is formed. In general, methylation reactions are assumed to be important and have been involved in all mechanistic proposals of MTO research thus far. Different methylation mechanisms have been examined; in particular a direct (concerted) and stepwise route

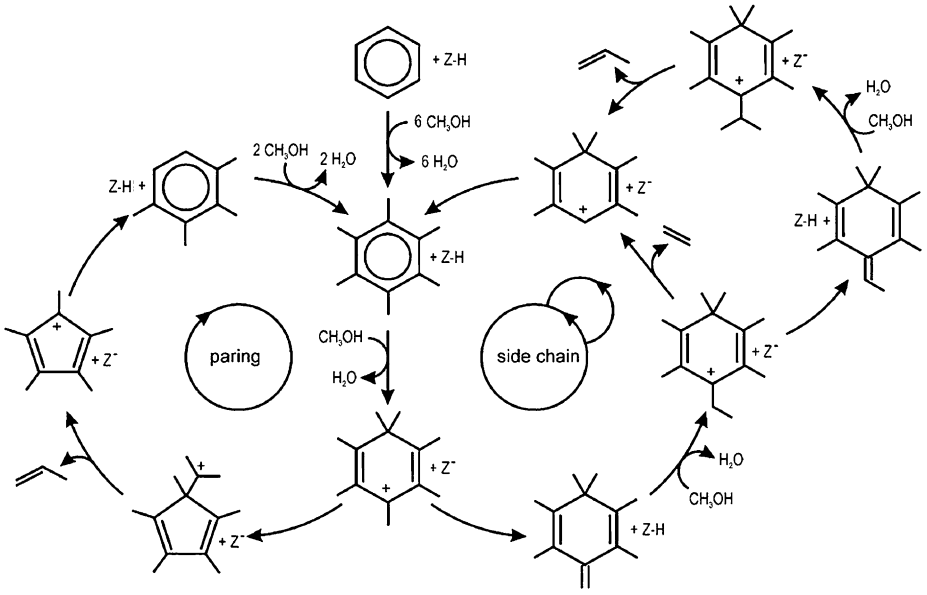

Figure 10. Overview of the paring and side-chain schemes for MTO conversion based on aromatic HP species. (Reprinted from ref. [46].)

have been distinguished.[127] So far, most theoretical studies have used the concerted mechanism, considering physisorbed methanol and the co-adsorbed alkene or aromatic in the nanoporous material. Using this approach, a good agreement between theoretical and experimental data was obtained for the methylation of alkenes in H-ZSM-5 (see Figure 5 and 6 in Section 2).[24,25] We refer to the work of Svelle and co-workers for an overview of different methylation mechanisms.[127] Experimental and theoretical studies involving aromatic HP intermediates have focused almost exclusively on the two mechanistic ideas illustrated in Figure 10 to determine the dominating mechanism.

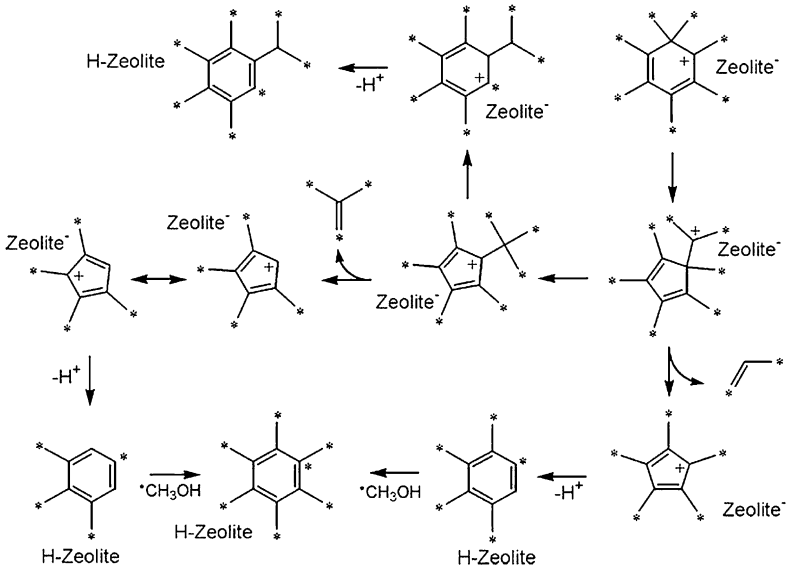

Figure 11. Paring type reaction, with indication of $^{12}C/^{13}C$ scrambling. (Reprinted with permission from ref. [131]. Copyright 2004 Elsevier.)

4.1.1. Aromatic-Based Cycles in H-SAPO-34

A catalytic study of Song et al. on H-SAPO-34 showed that both the reactivity of PMBs and the selectivity toward propene formation increase with the number of methyl substituents.[109] In particular, they reported that xylenes and trimethylbenzenes lead mostly to ethene formation, while higher tetra- to hexamethylbenzenes are responsible for propene production.[109] The role of hexamethylbenzene (HMB) as crucial HP species in H-SAPO-34 has been confirmed, and this compound has been identified through various experimental techniques.[107,128,129] Theoretical DFT-based studies, both using periodic unit cells[130] and extended clusters,[119] have confirmed the influence of the number of methyl groups on PMBs. Haw and co-workers indicated that in addition to PMBs, methylnaphthalenes can also act as active HP species, thereby exhibiting a high selectivity for ethene.[109,110] This could be related to the observation that methylnaphthalenes never contain more than four methyl groups.[96]

Initial mechanistic investigations used pulse experiments with labeled methanol over H-SAPO-34 and revealed carbon-label scrambling in the produced olefins and encapsulated HP species.[109,128] This exchange between ring ^{12}C and methyl ^{13}C carbon atoms is believed to be indicative for a paring type mechanism, as can be understood from Figure 11.[109,131] However, this suggestion must be carefully considered since experimentally estimated scrambling rates show that label incorporation occurs very fast at high temperatures.[67,131] Theoretical investigations of Arstad et al. using first-principle calculations, both in the gas phase and using a small zeolite cluster model, explored the possibilities of olefin formation by ring expansion and contraction reactions.[64,65] They also found that scrambling reactions of benzenium ions with ethyl or isopropyl groups are initiated by a ring expansion to a seven-membered ring, which can rearrange to the original benzenium compound.[66] Previously, the same researchers investigated alkene addition and elimination from the ethyl- or (iso)propylmethylbenzenes on small zeolite cluster models.[67,132] Their calculations confirmed the higher activity and propene selectivity for higher methylated benzene compounds, as experimentally observed. Furthermore, these two studies clearly show that carbon-atom scrambling and alkene formation in the MTO conversion can take place via the same intermediates.

Although these theoretical studies provide good insight into the reactivity of possible HP intermediates, the zeolitic environment should be taken into account since interactions between the organic HP species and the inorganic framework, as well as steric limitations, might be crucial for the detailed reaction mechanism. Wang et al. investigated the side-chain and paring cycles starting from HMB within H-SAPO-34 using periodic DFT calculations. They report that the side-chain cycle only yields propene, since a very high barrier is found for the ethene elimination.[63] Notably, these authors modeled the ethene elimination through a β-hydride shift or with a spiro intermediate as depicted in Figure 12 (routes A and B). In their analysis of the paring cycle, the regeneration of methylbenzenes from five-membered ring cations is the major bottleneck. The overall barriers for this cycle are higher than for the side-chain mechanism, leading to the conclusion that the paring scheme is less important in H-SAPO-34.[133]

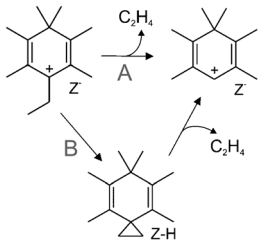

Figure 12. Suggested reactions for ethene elimination through a hydride shift (A) and a two-step mechanism via a spiro intermediate (B).[63]

4.1.2. Aromatic-Based Cycles in H-Beta

As mentioned above, zeolite H-Beta has also been studied since its spacious pores drastically limit steric hindrance, and hence additional insight on important HP intermediates can be obtained.[111,113,126,131] In particular, the heptamethylbenzium cation (heptaMB$^+$) appears to be the most active aromatic HP compound.[112,115,134,135] Due to its high proton affinity (see Table 1), HMB is typically methylated by methanol[136] and the resulting heptaMB$^+$ cation can be observed by NMR[112] and UV/Vis[115] spectroscopy. This reaction was extensively studied by Lesthaeghe and co-workers in the CHA, BEA, and MFI topologies.[137] The following order of reactivity was obtained: CHA $\gg$ MFI $>$ BEA. The corresponding transition states of the *ipso*-methylation of HMB are depicted in Figure 13. The CHA cage offers an ideal electrostatic surrounding for the organics occluded in the zeolitic materials, compared to MFI and BEA. Clearly, these findings strongly depend on the particular HP species.

4.1.3. Aromatic-Based Cycles in H-ZSM-5

Most theoretical studies on active MTO routes have focused on H-ZSM-5. Both the side-chain and paring mechanism were investigated by means of DFT computations using extended finite clusters. In a joint experimental/theoretical effort, McCann et al. reported the first complete catalytic route for MTO conversion (Figure 14).[77] The authors explained the formation of isobutene through a paring mechanism by connecting toluene to the experimentally observed 1,1,2,4,6-pentamethylbenzenium and 1,3-dimethylcyclopentadienylium cations.[114,138] In this paring route the initial *ipso*-methylation of toluene is the rate determining step. This is not the case for an investigated side-chain route starting from *ortho*-xylene—see Figure 15—which exhibits a difficult ethene split-off, with barriers of approximately 200 kJ mol^{-1}.[46] Note that these investigated mechanisms start from lower methylated PMBs, following the experimental observations that these HP species are the most active in H-ZSM-5 (Section 3).[135,139–142] Moreover, theoretical calculations could clarify the importance of transition-state-shape selectivity, as from durene on the transition state for an *ipso*-methylation lacks space at the channel intersections of H-ZSM-5.[137] Chan and Radom used DFT computations on 5T clusters and reported favorable transition states for olefin production.[143] To date, further simulations accounting for the zeolite framework are missing, and at this point there is no conclusive theoretical evidence for a side-chain aromatic-based route in H-ZSM-5. However, the mechanism cannot be disregarded considering the original experiments of Mole[101,102] as well as in situ NMR experiments.[93] The observed product distribution of H-ZSM-5 could not be explained based on an aromatic HP, and hence further investigations were needed.

4.2. The Dual Cycle Concept: Aromatics versus Alkenes

While PMBs emerged as the most important HP species in H-SAPO-34 and H-Beta, in the archetypal H-ZSM-5 catalyst

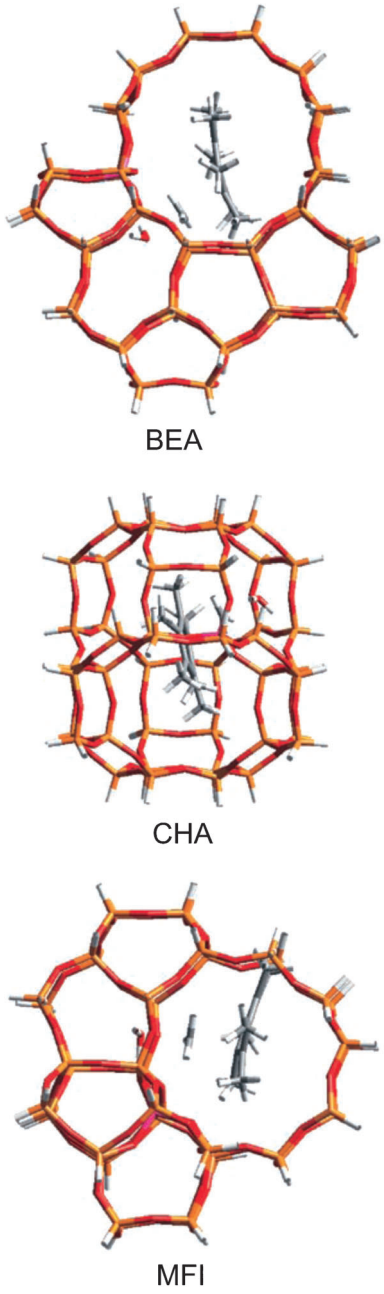

Figure 13. Transition state geometries for the formation of the heptaMB$^+$ cation in BEA, CHA, and MFI topologies. The Figure shows the large clusters used to represent the zeolite environment; 52T, 44T, and 46T for BEA, CHA and MFI, respectively. (Reprinted from ref. [137].)

a somewhat different behavior has been observed. In particular, Svelle and co-workers found that ethene and propene are reactive when co-fed with methanol on H-ZSM-5,[12,13] in contrast to the H-SAPO-34 catalyst.[104,105]

In a more detailed study using ^{13}C labeling, Svelle et al. observed two distinct product groups, as shown in Figure 16.[14,144] The distinctly different degree of ^{13}C incorporation in ethene on the one hand, and propene and higher alkenes on the other hand led to the conclusion that a different mechanism must lie at the basis of the product formation. Based on these observations, the authors proposed a complete

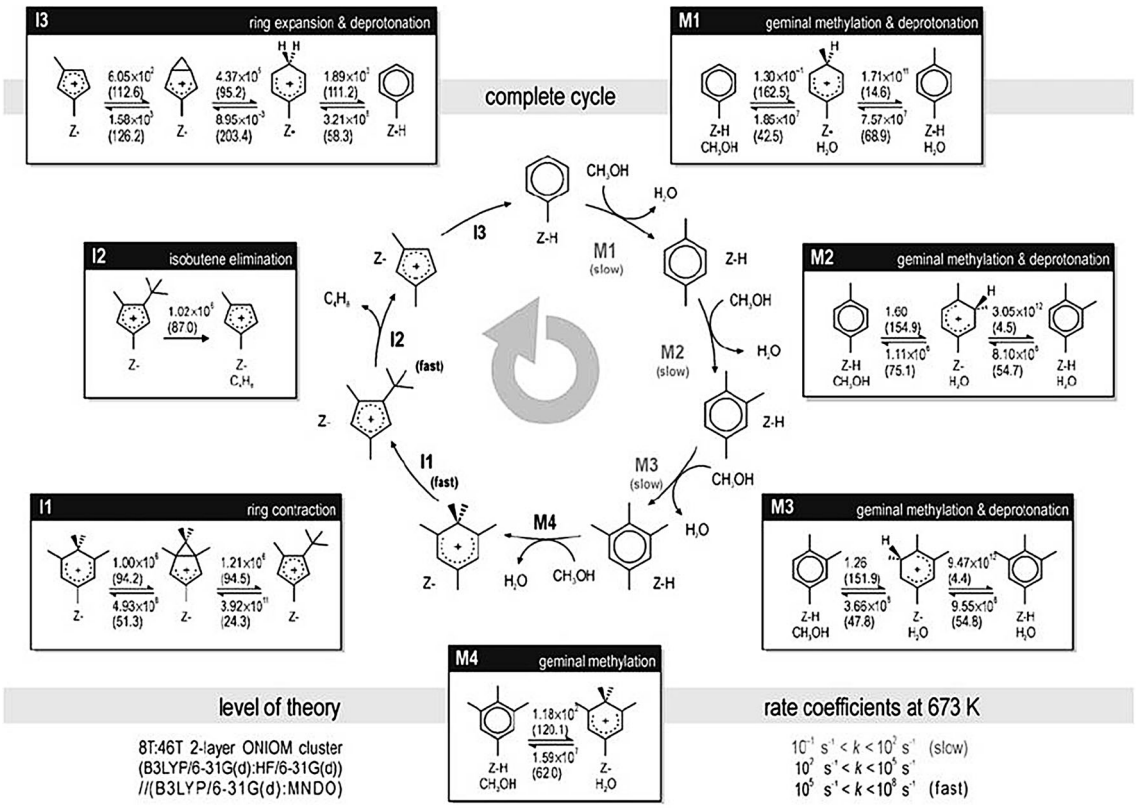

Figure 14. Full catalytic cycle for carbon-atom scrambling and isobutene formation from methanol through a combined methylbenzene/cyclopentenyl cation pool—involving the paring mechanism—in H-ZSM-5.[77] Calculated intrinsic rate coefficients [s] calculated at 673 K along with intrinsic reaction barriers [kJ mol^{-1}] at 0 K (in brackets) are given. The calculations relate to 8T:46T ONIOM computations; in particular B3LYP/6-31G(d):HF/6-31G(d) energy simulations on B3LYP/6-31G(d):MNDO optimized geometries. (Reprinted from ref. [77].)

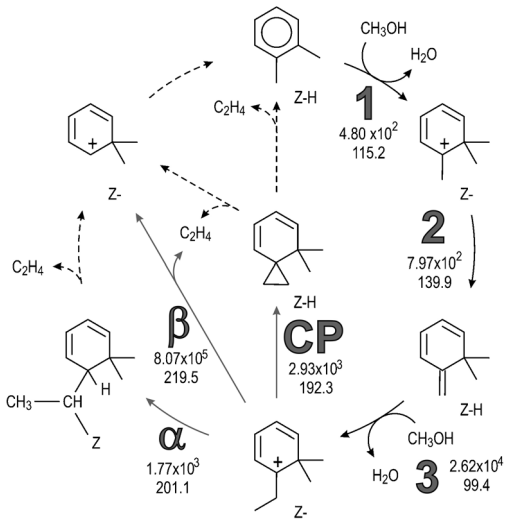

Figure 15. Mechanistic proposal for full side-chain elimination for the formation of ethene from orhoxylene in H-ZSM-5.[46] 1) gem-methylation; 2) deprotonation to exocyclic double bond; 3) side-chain methylation. Three possible routes provide ethene, from the left inwards: double α-hydride shift, single β-hydride shift, and deprotonation to a cyclopropyl (CP) intermediate. Calculated intrinsic rate coefficients [s] calculated at 673 K (top) along with intrinsic reaction barriers [kJ mol^{-1}] at 0 K (bottom) are given. The calculations relate to 8T:46T ONIOM computations; in particular B3LYP/6-31G(d):HF/6-31G(d) energy simulations on B3LYP/6-31G(d):MNDO optimized geometries. (Reprinted from ref. [46].)

dual cycle mechanism for MTO conversion in H-ZSM-5, consisting of a polymethylbenzene cycle predominantly yielding ethene and an autocatalytic alkene cycle yielding mostly propene and higher alkenes. Co-reaction experiments (^{12}C *p*-xylene and ^{13}C methanol) conducted at high feed rates revealed that the aromatics-based route produces ethene and propene at similar rates; whereas, the alkene route contributes insignificantly to ethene, but is a highly relevant mode of propene formation for H-ZSM-5.[142] Figure 17 illustrates the interconnection between these cycles: the polymethylbenzene cycle may also produce limited amounts of propene, which can act directly as a co-catalyst in the alkene cycle, while alkenes undergoing secondary reactions (oligomerization and cyclization) result in additional polymethylbenzene species. The suggested alkene methylation and cracking route bears resemblance to the original autocatalytic mechanism proposed by Dessau et al.,[99,100] with the notable exception that in Svelle's view ethene does not take part in the alkene cycle. In the dual cycle model, ethene and propene formation are mechanistically separated, which opens promising perspectives of eventually allowing a greater control over the ethene-to-propene product ratio obtained from MTO conversion.[135]

The observations leading to the dual cycle proposal have been corroborated by theoretical studies. Lesthaeghe et al. investigated a possible alkene route for MTO conversion, illustrated in Figure 18.[145] The authors obtained reaction barriers

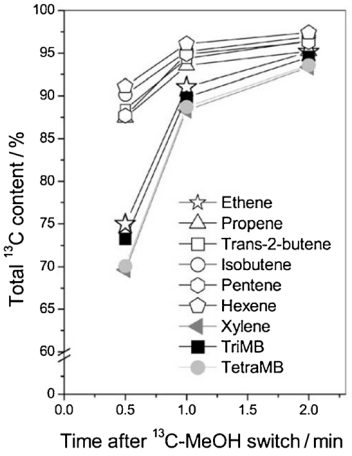

Figure 16. Total ^{13}C content in the effluent compounds after 18 min of ^{12}C methanol reaction followed by a switch to ^{13}C methanol and further reaction for 0.5, 1.0 and 2.0 min at 623 K. (Reprinted with permission from ref. [144]. Copyright 2007 Elsevier.)

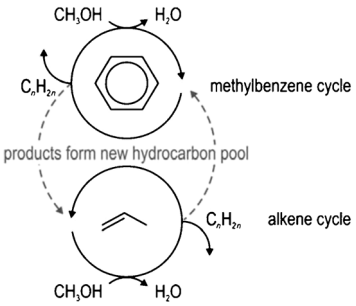

Figure 17. Dual cycle mechanism for MTO conversion in H-ZSM-5. (Reprinted from ref. [145].)

for chain growth by methylation of 60–80 kJ mol^{-1}, similar to those previously reported for the methylation of HMB in H-SSZ-13 (see Figure 13) and the methylation of lower methylbenzenes in H-ZSM-5.[137] For the cracking steps barriers of 70–120 kJ mol^{-1} were found, with reactions leading to propene displaying generally lower barriers than those producing ethene, in agreement with the experimentally observed favoring of propene production.[14, 144]

4.3. Other Zeolite Materials as MTO Catalysts

By varying the catalyst topology and/or composition in a controlled manner, more mechanistic information on possible MTO routes can be obtained. Table 2 presents a selection of zeolitic materials tested for MTO conversion. Notably, most materials were included in the work of Olsbye and co-workers, who also reported their corresponding compositions.[2] We list in Table 2 the available space, defined as the maximum volume of a sphere that can be included in the porous material[27] as it provides an indication of the size of possible HP intermediates that fit into the cage. The maximum diameter of a sphere that can be included in the micropore system also plays a crucial role in product selectivity, and the materials are listed according to this parameter, differentiating between

Table 2. Topologies and materials tested for MTO conversion.

Topology	Material	Maximum Ring Size	Maximum diameter [Å]
BEA	Beta	12-rings	6.68
AFS	SAPO-46		9.51
OFF	*Offrerite*		*7.00*
AFI	*SAPO-5*		*8.30*
MFI	ZSM-5	10-rings	6.36
MEL	ZSM-11		7.72
TUN	TNU-9		8.46
IMF	IM-5		7.34
FER	ZSM-35		6.31
TON	*ZSM-22*		*5.71*
MTT	*ZSM-23*		*6.19*
**MRE*	*ZSM-48*		*6.36*
EUO	*EU-1*		*7.00*
AEL	SAPO-11		5.64
AFO	*SAPO-41*		*5.43*
CHA	SAPO- 34, SSZ-13	8-rings	7.37
ERI	UZM-12		7.04
LTA	UZM-9		11.05
UFI	UZM-5		10.09
RTH	RUB-13		8.18
DDR	ZSM-58		7.66
AEI	SAPO-18		7.33
LEV	SAPO-35		7.10

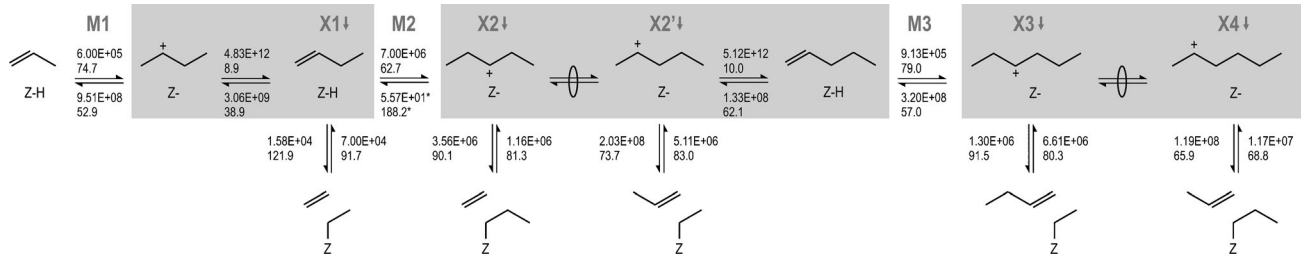

Figure 18. Suggested full alkene-based route for MTO conversion in H-ZSM-5, from ref. [145]. Methylation steps (M1–M3, depicted horizontally) and cracking steps (X1–X4, depicted vertically) are shown. Calculated intrinsic rate coefficients [s] calculated at 673 K (top) along with intrinsic reaction barriers [kJ mol^{-1}] at 0 K (bottom) are given. The calculations relate to 8T:46T ONIOM computations; in particular B3LYP/6-31G(d):HF/6-31G(d)-D energy simulations on B3LYP/6-31G(d):MNDO optimized geometries. (Reprinted from ref. [145].)

large-, medium-, and small-pore materials with 12-, 10-, and 8-ring pore windows, respectively. Some materials (expressed in italics in Table 2) correspond to 1D channel systems.

A detailed overview of all studies discussing new materials for MTO conversion is beyond the scope of this work. Many studies focus on varying process parameters and little information is revealed on the underlying reaction mechanisms, however, some did emphasize on obtaining mechanistic information. A prominent example is the study by Cui et al., investigating the MTO activity of four framework structures—H-ZSM-22 (TON: 1D), H-SAPO-34 (CHA: 3D), H-ZSM-11 (MEL: 3D), and H-SAPO-5 (AFI: 1D)—using GC analysis.[18] The narrow 1D channels in the case of H-ZSM-22 (see Figure 3) cannot accommodate the aromatic MTO intermediates, and hence this catalyst fails to produce ethene. The same topology (TON), in the KZ-2 material, was earlier studied by Parker and Bibby, leading to the same conclusion.[146] The transition state selectivity encountered in H-ZSM-22 does not take place in the case of an AFI topology, since this topology has much larger 1D channels (see Figure 3). However, Teketel et al. later showed that one must be careful to draw general conclusions, reporting that under suitable reaction conditions—low feed rates and reaction temperatures between 400 and 500 °C—H-ZSM-22 is as active as H-SAPO-34, with the product stream containing mainly branched (C_{5+}) alkenes, resulting from an alkene-based active route.[147] A series of 1D 10-ring pore zeolites with small differences in the channel shape and dimensions has also been examined, in particular zeolites H-ZSM-22, H-ZSM-23, H-ZSM-48, and H-EU-1.[148] Except for EU-1, all catalysts gave high selectivity for (C_{5+}) hydrocarbons. Unlike ZSM-22 and ZSM-23, the EU-1 and ZSM-48 catalysts displayed notable amounts of aromatics in their (C_{5+}) fraction.

Bleken et al. investigated a series of 3D 10-ring zeolites with varying size of channel intersections: TNU-9 (TUN) and IM-5 (IMF) exhibit larger cavities compared to ZSM-5 (MFI) and ZSM-11 (MEL).[141] These materials show a very similar effluent selectivity, whereas the underlying reaction mechanism differs due to the topological features.[141] IM-5 has been previously compared to ZSM-5 by Zones et al., who reported that the product spectrum of the aromatics is shifted towards heavier compounds.[149] Zeolite H-ZSM-11 has also been investigated by other researchers, pointing out the similarity with H-ZSM-5 for its catalytic properties.[150,151] The DDR topology—also shown in Figure 3—has been studied as MTO catalyst: Kumita et al. reported the high selectivity for small olefins (no longer than C_4) of the H-ZSM-58 material.[152] The good catalytic performance of ZSM-34, in both its protonated[153] and hetero-atom exchanged[154] forms, was demonstrated as well. This material is a more complex ERI/OFF intergrowth structure and the small pores result in a high selectivity toward ethene and propene.[153,154]

While high-silica materials often provide a high thermostability, different aluminophosphates (AlPOs) have also been examined in recent years. SAPO-11 (AEL), SAPO-18 (AEI), and SAPO-35 (LEV) have been compared with SAPO-34.[155,156] Dai et al. reported on the distinct catalytic MTO performance of silicoaluminophosphate materials with different topologies, in particular SAPO-34, SAPO-41, SAPO-11, and SAPO-46; the obtained product distributions are displayed in Figure 19.[157] The authors highlight the promising behavior of H-SAPO-41. UV/Vis measurements reveal that this material contains similar aromatic HP species as H-SAPO-34.

5. Deactivation by Coke Formation: Passive Routes

Sections 3 and 4 show that carbonaceous species, mainly aromatics or alkenes, are present in the zeolite pores and/or intersections, and that these compounds form the HP responsible for olefin elimination. However, these intermediates can also transform into larger compounds, so-called coke species, and hence lead to the highly undesirable catalyst deactivation. This deactivation is due to pore blocking or poisoning of the acid sites. Chen et al. reviewed the diffusion, coke formation, and deactivation on SAPO type catalysts, focusing on the influence of crystal size and operating temperatures.[4] The coking behav-

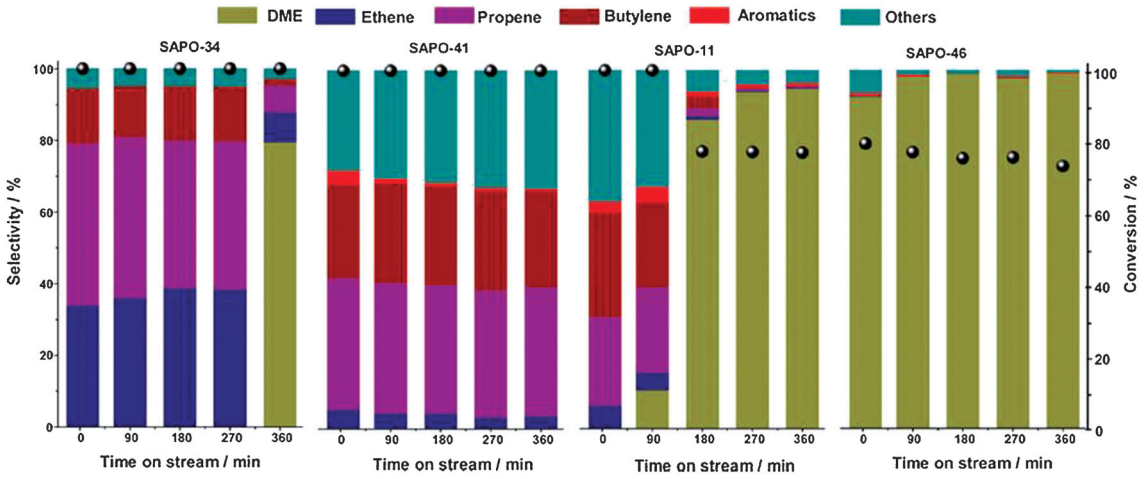

Figure 19. Conversion and product distribution of different SAPO materials for MTO reaction at 723 K up to a time-on-stream of 6 h. (Reprinted with permission from ref. [157]. Copyright 2011 American Chemical Society.)

ior also crucially depends on both the catalyst topology and acidity. The influence of acidity has been assessed by varying the Si/Al ratio of H-ZSM-5 crystals[158] or by varying the chemical composition, for example, through comparison of H-SAPO-34 and its more acidic aluminosilicate variant H-SSZ-13.[62,81,119,159] Using theoretical DFT-based simulations, these authors highlighted the dual role of bicyclic compounds in MTO catalysts with CHA topology.[62,79] Naphthalenic species can grow by methylation, as depicted in Figure 20, however particular trimethylated species should be regarded as coke precursors rather than as active HP species, as the side-chain methylation reaction starting from a trimethylated naphthalenium cation was found to be very slow.[62,79] These conclusions hold for the isostructural H-SAPO-34 and H-SSZ-13 materials. Theoretical activation barriers of methylations are typically 25 kJ mol^{-1} lower for H-SSZ-13 than H-SAPO-34.[62,79] This conclusion can be generalized for methylations at larger aromatics in CHA-type catalysts.[119] Based on both computed and experimental IR spectra of methanol and ethanol conversion over H-SAPO-34, the typical coke band found slightly above 1600 cm^{-1} could be explicitly assigned to large methylated aromatic cations entrapped in the catalyst pores.[81] In a combined theoretical/experimental effort the non-systematic role of the methyl positions was highlighted. Depending on the precise position of methyl groups, some naphthalenic species were found to be equally active towards methylation. The overall activity is nevertheless dictated by the subsequent reaction.[119]

The obtained results are in line with those of Bleken et al.[159] H-SSZ-13 and H-SAPO-34 perform similarly in MTO, however, a lower optimal operation temperature and increased ethene/propene ratio were found for HSSZ-13.[159] In situ MAS NMR-UV/Vis data indicated a decrease of the mean number of methyl groups per aromatic rings with deactivation, which might explain the change of product selectivity from propene to ethene.[160] Hereijgers et al., however, reported that product-state selectivity is dominating the reaction outcome and influences the selectivity in the case of deactivated H-SAPO-34.[128] Dai et al. also observed the formation of polyaromatic coke species using ^{1}H MAS NMR and in situ UV/Vis spectroscopy for other SAPO-type materials.[32,157] In particular, GC-MS analysis of the organic species formed in the SAPO materials revealed that for SAPO-34, the main species is naphthalene, for SAPO-41 and SAPO-11 tetraMBs and for SAPO-46 the amount of large aromatics is negligible. Overall, the formed aromatics are held responsible for pore blockage and hence deactivation of the SAPO-34 catalyst.[128] Wei and co-workers very recently reported the importance of non-aromatic diamondoid hydrocarbons, in particular adamantane, as new type of coke precursors for methanol conversion over SAPO-type materials at low reaction temperatures.[161] In summary, although many experimental observations are available, a detailed reaction mechanism for coke formation in small-pore zeolites is still missing and research is ongoing.

The essential influence of topology on the type of deactivated products can be assessed by comparing H-ZSM-5 with H-SAPO-34. Coke formation in the case of H-ZSM-5 has been related to the growth of large aromatic species at channel intersections[144] and/or formation of graphitic coke at the outer surface of the zeolite crystals;[162] whereas for H-SAPO-34 polyaromatics trapped in the pores are responsible for the deactivation[163–165]. Mores et al. used in situ UV/Vis spectroscopy combined with confocal fluorescence microspectroscopy to support these findings. They reported that aromatic coke compounds are mainly formed inside the crystals, whereas graphitic coke on H-ZSM-5 crystals is initially formed at the edges of the crystal.[22] A significant decrease in the formation of graphite-like coke species was found for ZSM-5 crystals with an external silicalite-1 layer compared with conventional ZSM-5 crystals. This decrease is due to the egg/yolk distribution of aluminum and the inactivity of the silicalite-1 layer towards coke formation.[166] The spatial distribution of bulkier hydrocarbons was recently examined using parent and steamed ZSM-5 samples as MTO catalysts. A core-shell distribution could be visualized for parent ZSM-5 as studied by scanning transmission X-ray spectroscopy (STXM). STXM allows constructing 2D maps of coke deposits by measuring in situ the carbon K-edge. It also allows for the differentiation between distinct carbon species.[167] Wragg et al. reported anisotropic changes in the unit-cell dimensions of H-SAPO-34 in the MTO process from

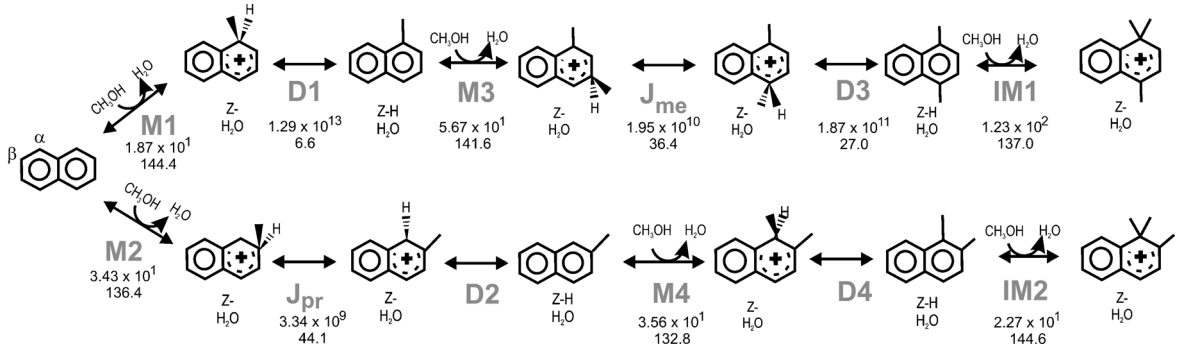

Figure 20. Growth of naphthalenic species by methylation in H-SAPO-34.[62] Methylations (M1–M4), deprotonations (D1–D4), methyl hop (J_{me}), proton hop (J_{pr}), and *ipso*-methylations (IM1–IM2) are shown. Calculated intrinsic rate coefficients [s] calculated at 670 K (top) along with intrinsic reaction barriers [kJ mol^{-1}] at 0 K (bottom) are given. The calculations relate to 6T:44T ONIOM computations; in particular B3LYP/6-31G(d):HF/6-31G(d)-D energy simulations on B3LYP/6-31G(d):MNDO optimized geometries. (Reprinted from ref. [62].)

powder XRD patterns.[168] The buildup of large coke species is held responsible for the observed prolongation of approximately 3% in the *c* axis (at 500 °C). Rapid, high-energy X-ray diffraction imaging was used to study a more industrial-like reactor, in particular a large (4 mm diameter) fixed MTO reactor bed in situ.[169] Reaction intermediates and coke species were tracked along the reactor bed. By means of a kinetic model, the formation of the HP species as well as a coke front could be explained; some regions of the catalyst bed clearly remain coke free.

To date, few suggestions have been made regarding the details of possible passive routes, that is, reaction mechanisms leading to the growth of coke species. Guisnet and Magnoux discussed the general chemistry of coke formation, pointing out the crucial role of reaction temperature and the involvement of hydrogen transfer, condensation, and rearrangement steps for the formation of (polyaromatic) coke at high temperatures (i.e. >350 °C).[170] Bjørgen and co-workers reported that for large-cavity catalysts (i.e. comprising pores defined by 12-rings) H-beta, H-MCM-22, and H-mordenite, large hexa-methylnaphthalene compounds could easily be formed from dihydrotrimethylnaphthalene by methylation reactions and hydrogen transfers as depicted in Figure 21, leading to fast deactivation.[134,171]

6. Conclusions and Outlook

In view of the rising interest in renewable resources, the MTO process is a timely subject as it is one of the most prominent technologies to bypass crude oil in the production of light olefins. This process has proven to be a showcase example where rational design of the catalyst is extremely difficult due to insufficient knowledge of the reaction mechanism. In this review, we highlighted spectroscopic and theoretical breakthroughs leading to the HP hypothesis, stating that organic compounds present in the inorganic framework co-catalyze the actual reactions. We emphasized the additional insight that can be gained from theoretical simulations, as these are able to compute the properties of individual reaction steps and can lead to the characterization of individual reaction intermediates. Computational modeling and spectroscopy have nowadays matured to a level where they can provide accurate and reliable data. The structure-activity relationship of the archetypal MTO catalysts, that is, H-ZSM-5 and H-SAPO-34, was reviewed. In summary, for a CHA-type topology, heavily methylated aromatics are found to be the most active HP compounds, leading to the production of both propene and ethene. Paring and side-chain reaction mechanisms have been proposed. In the case of the MFI topology, an interconnected dual cycle mechanism was found, since both alkenes and (lower methylated) aromatics play an active role in olefin production. From this review, it is evident that many puzzling questions regarding the ongoing reaction mechanisms of the MTO process remain unanswered. However, developments in experimental setups and theoretical methodologies continue to offer new possibilities and clearly this process will keep challenging both experimental and theoretical researchers for many years.

A first attractive perspective is offered by hierarchically structured zeolites, containing pore systems of different sizes, which are a rather new class of catalytic materials.[172] The introduction of mesopores enhances the overall diffusivity of molecules toward and away from the catalytically active sites and/or alters the acid properties. Bjørgen et al. demonstrated an improved catalytic MTO performance for H-ZSM-5 zeolite containing mesopores introduced through treatment with NaOH.[173] Mei et al. investigated a similar material for the MTP reaction, reporting high propylene selectivity (42.2%) and propylene/ethylene ratio (10.1).[174] The enhanced catalytic behav-

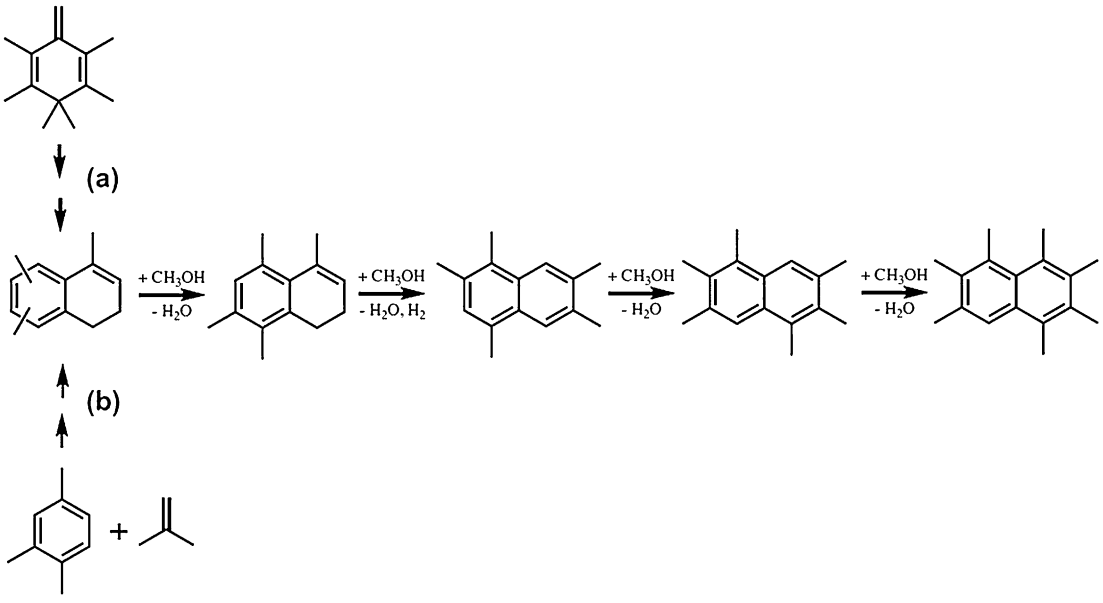

Figure 21. Mechanistic proposal for the formation of heptaMN through the dihydrotriMN intermediate in large-cavity catalysts. (Reprinted with permission from ref. [134]. Copyright 2010 Elsevier.)

ior does not necessarily result from the presence of mesopores in the zeolite samples, as has also been indicated by the authors. This was confirmed by Sommer et al. for H-SSZ-13, reporting that mesopores do not lead to an improvement of the catalytic MTO properties.[175] The zeolite samples containing mesopores showed a decreased methanol conversion capacity presumably due to a decreased surface area and number of acid sites. Recent advances allow for the synthesis of zeolites with pores of different dimensions, for example, the ITQ-39 zeolite with intersecting medium (10-rings) and large (12-rings) pores connected.[176–178] These materials have shown interesting properties to convert gasoline into diesel by alkylation. In an analogous way, hierarchically structured materials might be of interest for MTO conversion.

Thus far, computational studies mainly employ idealized models of the MTO catalyst (see Section 3). However, the importance of framework defects on the structure-activity relationship for MTH chemistry and the desilication process has recently been demonstrated for ZSM-5 zeolites.[179–181] Barbera et al. pointed towards the crucial role of internal silanol groups for the deactivation behavior of the catalyst materials, whereas the activity typically depends on the acid site density.[181] Modeling defects in zeolites is hence a challenging topic and will benefit from advances in modeling techniques as large supercells would be needed to model these effects.

One of the most promising directions in zeolite modeling is the use of molecular dynamics (MD) simulations as these can account for framework flexibility and important entropy and temperature effects. Recent studies pointed out the importance of the framework flexibility of zeolites.[182–185] The influence of additional molecules, such as methanol or water, in a zeolitic host can also be modeled using MD simulations. To simulate chemical reactions taking place in a complex molecular environment some promising techniques, such as transition path sampling (TPS), have been developed.[186] Using TPS, reaction paths or trajectories are generated between specified reactants and products of the investigated reaction such that new reaction mechanisms can be discovered without prior knowledge of the transition states.[187,188] The application to nanoporous materials is, however, not straightforward. If the reaction coordinate of the reaction of interest is well-defined, simulations based on metadynamics can be performed to reconstruct the corresponding free energy landscape.[189–193] During a metadynamics simulation, the minima of the free energy landscape of the investigated system are filled with Gaussian functions to accelerate the sampling of a rare event. The determination of reliable kinetic coefficients based on the free energy profile obtained with metadynamics is challenging and currently under investigation in our research group. MD studies of direct relevance for the MTO process are scarce, and remain computationally demanding. However, this field will definitely benefit from new model developments and will gain a lot of interest in the near future. Recent studies by Hafner and co-workers demonstrate the importance of entropic effects and the need to account for the framework flexibility of zeolites by using large periodic models for reactions of hydrocarbons in zeolites.[194–197] Bai et al. performed MD simulations with the ReaxFF force field and were able to elucidate several reaction pathways of the MTO reaction in H-ZSM-5.[198] Furthermore, MD simulations can also aid the interpretation of experimental spectra, such as IR and UV/Vis since the behavior of a real catalytic material and the intermediates present within can be modeled. We have been applying MD simulations to generate a large set of conformations and combined them with time-dependent DFT to simulate absorption spectra of aromatic HP compounds.[199] These simulated data can serve as a benchmark to characterize absorption peaks of in situ UV/Vis spectra taken during the MTO reaction over CHA-type catalyst materials.

Another approach to boost mechanistic insights in MTO conversion may be expected from research focusing on new HP species, such as radicals. Catalytic routes studied thus far involve carbocationic intermediates. However, electron spin resonance (ESR) evidence was recently provided for the occurrence of the hexamethylbenzenium radical as a true reaction intermediate during the MTO reaction in SSZ-13 and SAPO-34.[200] ESR techniques applied by Madeira et al. revealed that radical species are formed during the ethanol-to-hydrocarbons reaction on H-ZSM-5.[201] Sommer et al. observed an enhanced catalytic MTO activity of H-SSZ-13 after neutron irradiation.[202] The presence of peroxy radicals and nonbridging oxygen-hole centers, introduced through bond rupture of the zeolitic framework, may alter the catalytic properties of the material. These radicals, characterized using ESR, showed a long-term stability, suggesting that neutron irradiation is a useful post-synthesis treatment which can modify the catalysts properties.[202] Due to their increased reactivity, radical intermediates are very likely to participate in the MTO conversion process, which open up a large series of new mechanistic routes.

Acknowledgements

We thank the Fund for Scientific Research Flanders (FWO), the Research Board of Ghent University, and BELSPO in the frame of IAP P7/05. Funding was also received from the European Research Council under the European Community's Seventh Framework Program [FP7(2007–2013) ERC grant agreement number 240483].

Keywords: ab initio calculations · chemical kinetics · heterogeneous catalysis · methanol-to-olefins process · reaction mechanisms

[1] Y. K. Park, C. W. Lee, N. Y. Kang, W. C. Choi, S. Choi, S. H. Oh, D. S. Park, *Catal. Surv. Asia* **2010**, *14*, 75.
[2] U. Olsbye, S. Svelle, M. Bjorgen, P. Beato, T. V. W. Janssens, F. Joensen, S. Bordiga, K. P. Lillerud, *Angew. Chem.* **2012**, *124*, 5910; *Angew. Chem. Int. Ed.* **2012**, *51*, 5810.
[3] S. Ilias, A. Bhan, *ACS Catal.* **2013**, *3*, 18.
[4] D. Chen, K. Moljord, A. Holmen, *Microporous Mesoporous Mater.* **2012**, *164*, 239.
[5] G. A. Olah, *Angew. Chem.* **2005**, *117*, 2692; *Angew. Chem. Int. Ed.* **2005**, *44*, 2636.
[6] G. A. Olah, *Angew. Chem.* **2013**, *125*, 112; *Angew. Chem. Int. Ed.* **2013**, *52*, 104.

[7] C. D. Chang, *Catal. Rev. Sci. Eng.* **1983**, *25*, 1.
[8] C. D. Chang, *Catal. Today* **1992**, *13*, 103.
[9] B. V. Vora, T. L. Marker, P. T. Barger, H. R. Nilsen, S. Kvisle, T. Fuglerud, *Stud. Surf. Sci. Catal.* **1997**, *107*, 87.
[10] H. Koempel, W. Liebner, *Stud. Surf. Sci. Catal.* **2007**, *167*, 261.
[11] J. F. Haw, W. Song, D. M. Marcus, J. B. Nicholas, *Acc. Chem. Res.* **2003**, *36*, 317.
[12] S. Svelle, P. O. Rønning, S. Kolboe, *J. Catal.* **2004**, *224*, 115.
[13] S. Svelle, P. Ronning, U. Olsbye, S. Kolboe, *J. Catal.* **2005**, *234*, 385.
[14] S. Svelle, F. Joensen, J. Nerlov, U. Olsbye, K.-P. Lillerud, S. Kolboe, M. Bjørgen, *J. Am. Chem. Soc.* **2006**, *128*, 14770.
[15] M. Bjorgen, K.-P. Lillerud, U. Olsbye, S. Svelle, Natural Gas Conversion Viii, Proceedings of the 8th Natural Gas Conversion Symposium, **2007**, 167, 463.
[16] D. M. Marcus, M. J. Hayman, Y. M. Blau, D. R. Guenther, J. O. Ehresmann, P. W. Kletnieks, J. F. Haw, *Angew. Chem.* **2006**, *118*, 1967; *Angew. Chem. Int. Ed.* **2006**, *45*, 1933.
[17] D. M. Marcus, K. A. McLachlan, M. A. Wildman, J. O. Ehresmann, P. W. Kletnieks, J. F. Haw, *Angew. Chem.* **2006**, *118*, 3205; *Angew. Chem. Int. Ed.* **2006**, *45*, 3133.
[18] Z.-M. Cui, Q. Liu, W.-G. Song, L.-J. Wan, *Angew. Chem.* **2006**, *118*, 6662; *Angew. Chem. Int. Ed.* **2006**, *45*, 6512.
[19] H. Yamazaki, H. Shima, H. Imai, T. Yokoi, T. Tatsumi, J. N. Kondo, *Angew. Chem.* **2011**, *123*, 1893; *Angew. Chem. Int. Ed.* **2011**, *50*, 1853.
[20] P. Magnoux, P. Roger, C. Canaff, V. Fouche, N. S. Gnep, M. Guisnet in *New Technique for the Characterization of Carbonaceous Compounds Responsible for Zeolite Deactivation, Vol. 34* (Eds.: B. Delmon, G. F. Froment), Elsevier, Amsterdam, **1987**, pp. 317.
[21] J. F. Haw, *Abstr. Pap. Am. Chem. Soc.* **1999**, *218*, U668.
[22] D. Mores, E. Stavitski, M. H. F. Kox, J. Kornatowski, U. Olsbye, B. M. Weckhuysen, *Chem. Eur. J.* **2008**, *14*, 11320.
[23] I. L. C. Buurmans, B. M. Weckhuysen, *Nat. Chem.* **2012**, *4*, 873.
[24] V. Van Speybroeck, J. Van der Mynsbrugge, M. Vandichel, K. Hemelsoet, D. Lesthaeghe, A. Ghysels, G. B. Marin, M. Waroquier, *J. Am. Chem. Soc.* **2011**, *133*, 888.
[25] S. Svelle, C. Tuma, X. Rozanska, T. Kerber, J. Sauer, *J. Am. Chem. Soc.* **2009**, *131*, 816.
[26] D. Lesthaeghe, University of Ghent, **2007**.
[27] http://www.iza-structure.org/databases.
[28] A. Corma, *Chem. Rev.* **1995**, *95*, 559.
[29] A. Zecchina, C. Lamberti, S. Bordiga, *Catal. Today* **1998**, *41*, 169.
[30] E. Stavitski, M. H. F. Kox, I. Swart, F. M. F. de Groot, B. M. Weckhuysen, *Angew. Chem.* **2008**, *120*, 3599; *Angew. Chem. Int. Ed.* **2008**, *47*, 3543.
[31] E. Stavitski, B. M. Weckhuysen, *Chem. Soc. Rev.* **2010**, *39*, 4615.
[32] W. Dai, N. Li, L. Li, N. Guan, M. Hunger, *Catal. Commun.* **2011**, *16*, 124.
[33] K. Suzuki, G. Sastre, N. Katada, M. Niwa, *Phys. Chem. Chem. Phys.* **2007**, *9*, 5980.
[34] K. Suzuki, G. Sastre, N. Katada, M. Niwa, *Chem. Lett.* **2007**, *36*, 1034.
[35] K. Suzuki, T. Noda, G. Sastre, N. Katada, M. Niwa, *J. Phys. Chem. C* **2009**, *113*, 5672.
[36] K. Suzuki, G. Sastre, N. Katada, M. Niwa, *Chem. Lett.* **2009**, *38*, 354.
[37] K. Suzuki, T. Nishio, N. Katada, G. Sastre, M. Niwa, *Phys. Chem. Chem. Phys.* **2011**, *13*, 3311.
[38] A. E. Alvarado-Swaisgood, M. K. Barr, P. J. Hay, A. Redondo, *J. Phys. Chem.* **1991**, *95*, 10031.
[39] S. R. Lonsinger, A. K. Chakraborty, D. N. Theodorou, A. T. Bell, *Catal. Lett.* **1991**, *11*, 209.
[40] A. Redondo, P. J. Hay, *J. Phys. Chem.* **1993**, *97*, 11754.
[41] R. Grau-Crespo, A. G. Peralta, A. R. Ruiz-Salvador, A. Gomez, R. Lopez-Cordero, *Phys. Chem. Chem. Phys.* **2000**, *2*, 5716.
[42] A. Bhan, Y. V. Joshi, W. N. Delgass, K. T. Thomson, *J. Phys. Chem. B* **2003**, *107*, 10476.
[43] J. Dědeček, D. Kaucký, B. Wichterlová, *Chem. Commun.* **2001**, *47*, 970.
[44] S. Sklenak, J. Dedecek, C. Li, B. Wichterlova, V. Gabova, M. Sierka, J. Sauer, *Angew. Chem.* **2007**, *119*, 7424; *Angew. Chem. Int. Ed.* **2007**, *46*, 7286.
[45] S. Sklenak, J. Dedecek, C. Li, B. Wichterlova, V. Gabova, M. Sierka, J. Sauer, *Phys. Chem. Chem. Phys.* **2009**, *11*, 1237.
[46] D. Lesthaeghe, A. Horre, M. Waroquier, G. B. Marin, V. Van Speybroeck, *Chem. Eur. J.* **2009**, *15*, 10803.
[47] T. Baba, N. Komatsu, Y. Ono, H. Sugisawa, *J. Phys. Chem. B* **1998**, *102*, 804.
[48] M. E. Franke, M. Sierka, U. Simon, J. Sauer, *Phys. Chem. Chem. Phys.* **2002**, *4*, 5207.
[49] J. A. Ryder, A. K. Chakraborty, A. T. Bell, *J. Phys. Chem. B* **2000**, *104*, 6998.
[50] P. Sarv, T. Tuherm, E. Lippmaa, K. Keskinen, A. Root, *J. Phys. Chem.* **1995**, *99*, 13763.
[51] U. Viswanathan, J. T. Fermann, L. K. Toay, S. M. Auerbach, T. Vreven, M. J. Frisch, *J. Phys. Chem. C* **2007**, *111*, 18341.
[52] C. Lo, B. Trout, *J. Catal.* **2004**, *227*, 77.
[53] H. O. Pastore, S. Coluccia, L. Marchese, *Annu. Rev. Mater. Res.* **2005**, *35*, 351.
[54] R. Vomscheid, M. Briend, M. J. Peltre, P. P. Man, D. Barthomeuf, *J. Phys. Chem.* **1994**, *98*, 9614.
[55] S. L. Suib, A. M. Winiecki, A. Kostapapas, *Langmuir* **1987**, *3*, 483.
[56] C. S. Blackwell, R. L. Patton, *J. Phys. Chem.* **1988**, *92*, 3965.
[57] C. Morterra, G. Magnacca, *Catal. Today* **1996**, *27*, 497.
[58] G. Sastre, D. W. Lewis, C. R. A. Catlow, *J. Phys. Chem. B* **1997**, *101*, 5249.
[59] D. Barthomeuf, *J. Phys. Chem.* **1993**, *97*, 10092.
[60] A. Buchholz, W. Wang, M. Xu, A. Arnold, M. Hunger, *Microporous Mesoporous Mater.* **2002**, *56*, 267.
[61] G. Sastre, D. W. Lewis, C. R. A. Catlow, *J. Mol. Catal. A Chem.* **1997**, *119*, 349.
[62] K. Hemelsoet, A. Nollet, V. Van Speybroeck, M. Waroquier, *Chem. Eur. J.* **2011**, *17*, 9083.
[63] C.-M. Wang, Y.-D. Wang, Z.-K. Xie, Z.-P. Liu, *J. Phys. Chem. C* **2009**, *113*, 4584.
[64] B. Arstad, S. Kolboe, O. Swang, *J. Phys. Org. Chem.* **2004**, *17*, 1023.
[65] B. Arstad, S. Kolboe, O. Swang, *J. Phys. Chem. A* **2005**, *109*, 8914.
[66] B. Arstad, S. Kolboe, O. Swang, *J. Phys. Org. Chem.* **2006**, *19*, 81.
[67] B. Arstad, J. B. Nicholas, J. F. Haw, *J. Am. Chem. Soc.* **2004**, *126*, 2991.
[68] B. Arstad, S. Kolboe, *J. Am. Chem. Soc.* **2001**, *123*, 8137.
[69] B. Arstad, S. Kolboe, *Catal. Lett.* **2001**, *71*, 209.
[70] S. R. Blaszkowski, M. A. C. Nascimento, R. A. van Santen, *J. Phys. Chem.* **1996**, *100*, 3463.
[71] S. R. Blaszkowski, R. A. van Santen, *J. Phys. Chem.* **1995**, *99*, 11728.
[72] S. R. Blaszkowski, R. A. van Santen, *J. Am. Chem. Soc.* **1997**, *119*, 5020.
[73] S. R. Blaszkowski, R. A. van Santen, *J. Phys. Chem. B* **1997**, *101*, 2292.
[74] A. Ghysels, D. Van Neck, V. Van Speybroeck, T. Verstraelen, M. Waroquier, *J. Chem. Phys.* **2007**, *126*, 224102.
[75] A. Ghysels, D. Van Neck, M. Waroquier, *J. Chem. Phys.* **2007**, *127*, 164108.
[76] A. Ghysels, V. Van Speybroeck, T. Verstraelen, D. Van Neck, M. Waroquier, *J. Chem. Theory Comput.* **2008**, *4*, 614.
[77] D. M. McCann, D. Lesthaeghe, P. W. Kletnieks, D. R. Guenther, M. J. Hayman, V. Van Speybroeck, M. Waroquier, J. F. Haw, *Angew. Chem.* **2008**, *120*, 5257; *Angew. Chem. Int. Ed.* **2008**, *47*, 5179.
[78] B. A. De Moor, A. Ghysels, M.-F. Reyniers, V. Van Speybroeck, M. Waroquier, G. B. Marin, *J. Chem. Theory Comput.* **2011**, *7*, 1090.
[79] K. Hemelsoet, A. Nollet, M. Vandichel, D. Lesthaeghe, V. Van Speybroeck, M. Waroquier, *ChemCatChem* **2009**, *1*, 373.
[80] M. Vandichel, D. Lesthaeghe, J. Van der Mynsbrugge, M. Waroquier, V. Van Speybroeck, *J. Catal.* **2010**, *271*, 67.
[81] K. Hemelsoet, A. Ghysels, D. Mores, K. De Wispelaere, V. Van Speybroeck, B. M. Weckhuysen, M. Waroquier, *Catal. Today* **2011**, *177*, 12.
[82] L. Goerigk, S. Grimme, *Phys. Chem. Chem. Phys.* **2011**, *13*, 6670.
[83] M. E. Foster, K. Sohlberg, *Phys. Chem. Chem. Phys.* **2010**, *12*, 307.
[84] J. Van der Mynsbrugge, K. Hemelsoet, M. Vandichel, M. Waroquier, V. Van Speybroeck, *J. Phys. Chem. C* **2012**, *116*, 5499.
[85] S. Grimme, *J. Comput. Chem.* **2004**, *25*, 1463.
[86] S. Grimme, J. Antony, T. Schwabe, C. Muck-Lichtenfeld, *Org. Biomol. Chem.* **2007**, *5*, 741.
[87] S. Grimme, J. Antony, S. Ehrlich, H. Krieg, *J. Chem. Phys.* **2010**, *132*, 154104.
[88] Y. Zhao, D. G. Truhlar, *Theor. Chem. Acc.* **2008**, *120*, 215.
[89] J.-D. Chai, M. Head-Gordon, *Phys. Chem. Chem. Phys.* **2008**, *10*, 6615.
[90] C. M. Nguyen, M. F. Reyniers, G. B. Marin, *J. Phys. Chem. C* **2011**, *115*, 8658.
[91] B. M. Weckhuysen, *Angew. Chem.* **2009**, *121*, 5008; *Angew. Chem. Int. Ed.* **2009**, *48*, 4910.

[92] M. Stöcker, *Microporous Mesoporous Mater.* **1999**, *29*, 3.
[93] W. Wang, A. Buchholz, M. Seiler, M. Hunger, *J. Am. Chem. Soc.* **2003**, *125*, 15260.
[94] S. Kolboe, *Acta Chem. Scand. Ser. A* **1986**, *40*, 711.
[95] S. Kolboe, *Stud. Surf. Sci. Catal.* **1988**, *36*, 189.
[96] J. F. Haw, D. M. Marcus, *Top. Catal.* **2005**, *34*, 41.
[97] D. Lesthaeghe, V. Van Speybroeck, G. B. Marin, M. Waroquier, *Angew. Chem.* **2006**, *118*, 1746; *Angew. Chem. Int. Ed.* **2006**, *45*, 1714.
[98] D. Lesthaeghe, V. V. Speybroeck, G. B. Marin, M. Waroquier, V. Van Speybroeck, *Ind. Eng. Chem. Res.* **2007**, *46*, 8832.
[99] R. M. Dessau, R. B. Lapierre, *J. Catal.* **1982**, *78*, 136.
[100] R. M. Dessau, *J. Catal.* **1986**, *99*, 111.
[101] T. Mole, G. Bett, D. Seddon, *J. Catal.* **1983**, *84*, 435.
[102] T. Mole, J. A. Whiteside, D. Seddon, *J. Catal.* **1983**, *82*, 261.
[103] B. E. Langner, *Appl. Catal.* **1982**, *2*, 289.
[104] I. M. Dahl, S. Kolboe, *Catal. Lett.* **1993**, *20*, 329.
[105] I. I. M. M. Dahl, S. Kolboe, *J. Catal.* **1994**, *149*, 458.
[106] I. M. Dahl, S. Kolboe, *J. Catal.* **1996**, *161*, 304.
[107] W. Song, J. F. Haw, J. B. Nicholas, C. S. Heneghan, *J. Am. Chem. Soc.* **2000**, *122*, 10726.
[108] W. Song, H. Fu, J. F. Haw, *J. Am. Chem. Soc.* **2001**, *123*, 4749.
[109] W. G. Song, H. Fu, J. F. Haw, *J. Phys. Chem. B* **2001**, *105*, 12839.
[110] H. Fu, W. Song, J. F. Haw, *Catal. Lett.* **2001**, *76*, 89.
[111] A. Sassi, M. A. Wildman, H. J. Ahn, P. Prasad, J. B. Nicholas, J. F. Haw, *J. Phys. Chem. B* **2002**, *106*, 2294.
[112] W. G. Song, J. B. Nicholas, A. Sassi, J. F. Haw, *Catal. Lett.* **2002**, *81*, 49.
[113] M. Bjorgen, U. Olsbye, S. Svelle, S. Kolboe, *Catal. Lett.* **2004**, *93*, 37.
[114] J. F. Haw, J. B. Nicholas, W. G. Song, F. Deng, Z. K. Wang, T. Xu, C. S. Heneghan, *J. Am. Chem. Soc.* **2000**, *122*, 4763.
[115] M. Bjørgen, F. Bonino, S. Kolboe, K.-P. Lillerud, A. Zecchina, S. Bordiga, *J. Am. Chem. Soc.* **2003**, *125*, 15863.
[116] M. Bjørgen, F. Bonino, B. Arstad, S. Kolboe, K.-P. Lillerud, A. Zecchina, S. Bordiga, *ChemPhysChem* **2005**, *6*, 232.
[117] J. Macht, R. T. Carr, E. Iglesia, *J. Am. Chem. Soc.* **2009**, *131*, 6554.
[118] S. Svelle, M. Bjørgen, *J. Phys. Chem. A* **2010**, *114*, 12548.
[119] V. Van Speybroeck, K. Hemelsoet, K. De Wispelaere, Q. Qian, J. Van der Mynsbrugge, B. De Sterck, B. M. Weckhuysen, M. Waroquier, *ChemCatChem* **2013**, *5*, 173.
[120] K. De Wispelaere, **2011**, Master Thesis, Ghent University.
[121] webbook.nist.gov.
[122] W. Wang, M. Hunger, *Acc. Chem. Res.* **2008**, *41*, 895.
[123] W. G. Song, D. M. Marcus, H. Fu, J. O. Ehresmann, J. F. Haw, *J. Am. Chem. Soc.* **2002**, *124*, 3844.
[124] Y. Jiang, W. Wang, V. R. R. Marthala, J. Huang, B. Sulikowski, M. Hunger, *J. Catal.* **2006**, *238*, 21.
[125] R. F. Sullivan, R. P. Sieg, G. E. Langlois, C. J. Egan, *J. Am. Chem. Soc.* **1961**, *83*, 1156.
[126] A. Sassi, M. A. Wildman, J. F. Haw, *J. Phys. Chem. B* **2002**, *106*, 8768.
[127] S. Svelle, M. Visur, U. Olsbye, Saepurahman, M. Bjorgen, *Top. Catal.* **2011**, *54*, 897.
[128] B. P. C. Hereijgers, F. Bleken, M. H. Nilsen, S. Svelle, K.-P. Lillerud, M. Bjørgen, B. M. Weckhuysen, U. Olsbye, *J. Catal.* **2009**, *264*, 77.
[129] W. Dai, M. Scheibe, N. Guan, L. Li, M. Hunger, *ChemCatChem* **2011**, *3*, 1130.
[130] C.-M. Wang, Y.-D. Wang, H.-X. Liu, Z.-K. Xie, Z.-P. Liu, *J. Catal.* **2010**, *271*, 386.
[131] M. Bjorgen, U. Olsbye, D. Petersen, S. Kolboe, *J. Catal.* **2004**, *221*, 1.
[132] B. Arstad, S. Kolboe, O. Swang, *J. Phys. Chem. B* **2004**, *108*, 2300.
[133] C.-M. Wang, Y.-D. Wang, H.-X. Liu, Z.-K. Xie, Z.-P. Liu, *Microporous Mesoporous Mater.* **2012**, *158*, 264.
[134] M. Bjørgen, S. Akyalcin, U. Olsbye, S. Benard, S. Kolboe, S. Svelle, *J. Catal.* **2010**, *275*, 170.
[135] S. Svelle, U. Olsbye, F. Joensen, M. Bjørgen, *J. Phys. Chem. C* **2007**, *111*, 17981.
[136] U. Olsbye, A. Virnovskaia, O. Prytz, S. J. Tinnemans, B. M. Weckhuysen, *Catal. Lett.* **2005**, *103*, 143.
[137] D. Lesthaeghe, B. De Sterck, V. Van Speybroeck, G. B. Marin, M. Waroquier, *Angew. Chem.* **2007**, *119*, 1333; *Angew. Chem. Int. Ed.* **2007**, *46*, 1311.
[138] T. Xu, D. H. Barich, P. W. Goguen, W. G. Song, Z. K. Wang, J. B. Nicholas, J. F. Haw, *J. Am. Chem. Soc.* **1998**, *120*, 4025.
[139] J. F. Haw, *Phys. Chem. Chem. Phys.* **2002**, *4*, 5431.
[140] J. Li, Y. Wei, G. Liu, Y. Qi, P. Tian, B. Li, Y. He, Z. Liu, *Catal. Today* **2011**, *171*, 221.
[141] F. Bleken, W. Skistad, K. Barbera, M. Kustova, S. Bordiga, P. Beato, K. P. Lillerud, S. Svelle, U. Olsbye, *Phys. Chem. Chem. Phys.* **2011**, *13*, 2539.
[142] M. Bjørgen, F. Joensen, K.-P. Lillerud, U. Olsbye, S. Svelle, *Catal. Today* **2009**, *142*, 90.
[143] B. Chan, L. Radom, *Can. J. Chem.* **2010**, *88*, 866.
[144] M. Bjorgen, S. Svelle, F. Joensen, J. Nerlov, S. Kolboe, F. Bonino, L. Palumbo, S. Bordiga, U. Olsbye, *J. Catal.* **2007**, *249*, 195.
[145] D. Lesthaeghe, J. Van der Mynsbrugge, M. Vandichel, M. Waroquier, V. Van Speybroeck, *ChemCatChem* **2011**, *3*, 208.
[146] L. M. Parker, D. M. Bibby, *Zeolites* **1983**, *3*, 8.
[147] S. Teketel, U. Olsbye, K. P. Lillerud, P. Beato, S. Svelle, *Microporous Mesoporous Mater.* **2010**, *136*, 33.
[148] S. Teketel, W. Skistad, S. Bernard, U. Olsbye, K. P. Lillerud, S. Svelle, *ACS Catal.* **2012**, *2*, 26.
[149] S. I. Zones, C. Y. Chen, A. Corma, M. T. Cheng, C. L. Kibby, I. Y. Chan, A. W. Burton, *J. Catal.* **2007**, *250*, 41.
[150] E. G. Derouane, P. Dejaifve, Z. Gabelica, J. C. Vedrine, *Faraday Discuss.* **1981**, *72*, 331.
[151] I. D. Harrison, H. F. Leach, D. A. Whan, *Zeolites* **1987**, *7*, 21.
[152] Y. Kumita, J. Gascon, E. Stavitski, J. a. Moulijn, F. Kapteijn, *Appl. Catal. A* **2011**, *391*, 234.
[153] F. Zhou, P. Tian, Z. Liu, G. Liu, F. Chang, J. Li, *Chin. J. Catal.* **2007**, *28*, 817.
[154] L. Zhang, C. Yang, X. Meng, B. Xie, L. Wang, L. Ren, S. Ma, F.-S. Xiao, *Chem. Mater.* **2010**, *22*, 3099.
[155] A. T. Aguayo, A. G. Gayubo, R. Vivanco, M. Olazar, J. Bilbao, *Appl. Catal. A* **2005**, *283*, 197.
[156] Z. D. Zhu, M. Hartmann, L. Kevan, *Chem. Mater.* **2000**, *12*, 2781.
[157] W. Dai, X. Wang, G. Wu, N. Guan, M. Hunger, L. Li, *ACS Catal.* **2011**, *1*, 292.
[158] D. Mores, J. Kornatowski, U. Olsbye, B. M. Weckhuysen, *Chem. Eur. J.* **2011**, *17*, 2874.
[159] F. Bleken, M. Bjorgen, L. Palumbo, S. Bordiga, S. Svelle, K.-P. Lillerud, U. Olsbye, *Top. Catal.* **2009**, *52*, 218.
[160] Y. Jiang, J. Huang, V. R. Reddy Marthala, Y. S. Ooi, J. Weitkamp, M. Hunger, *Microporous Mesoporous Mater.* **2007**, *105*, 132.
[161] Y. Wei, J. Li, C. Yuan, S. Xu, Y. Zhou, J. Chen, Q. Wang, Q. Zhang, Z. Liu, *Chem. Commun.* **2012**, *48*, 3082.
[162] D. M. Bibby, R. F. Howe, G. D. McLellan, *Appl. Catal. A* **1992**, *93*, 1.
[163] D. Chen, H. P. Rebo, K. Moljord, A. Holmen, *Ind. Eng. Chem. Res.* **1997**, *36*, 3473.
[164] A. T. Aguayo, A. E. S. del Campo, A. G. Gayubo, A. Tarrio, J. Bilbao, *J. Chem. Technol. Biotechnol.* **1999**, *74*, 315.
[165] D. Chen, H. P. Rebo, K. Moljord, A. Holmen, *Ind. Eng. Chem. Res.* **1999**, *38*, 4241.
[166] D. Mores, E. Stavitski, S. P. Verkleij, A. Lombard, A. Cabiac, L. Rouleau, J. Patarin, A. Simon-Masseron, B. M. Weckhuysen, *Phys. Chem. Chem. Phys.* **2011**, *13*, 15985.
[167] L. R. Aramburo, E. de Smit, B. Arstad, M. M. van Schooneveld, L. Sommer, A. Juhin, T. Yokosawa, H. W. Zandbergen, U. Olsbye, F. M. F. de Groot, B. M. Weckhuysen, *Angew. Chem.* **2012**, *124*, 3676; *Angew. Chem. Int. Ed.* **2012**, *51*, 3616.
[168] D. S. Wragg, R. E. Johnsen, M. Balasundaram, P. Norby, H. Fjellvåg, A. Grønvold, T. Fuglerud, J. Hafizovic, Ø. B. Vistad, D. Akporiaye, *J. Catal.* **2009**, *268*, 290.
[169] D. S. Wragg, M. G. O. Brien, F. L. Bleken, M. Di Michiel, U. Olsbye, H. Fjellvag, *Angew. Chem.* **2012**, *124*, 8080; *Angew. Chem. Int. Ed.* **2012**, *51*, 7956.
[170] M. Guisnet, *Appl. Catal. A* **2001**, *212*, 83.
[171] M. Bjorgen, U. Olsbye, S. Kolboe, *J. Catal.* **2003**, *215*, 30.
[172] S. Lopez-Orozco, A. Inayat, A. Schwab, T. Selvam, W. Schwieger, *Adv. Mater.* **2011**, *23*, 2602.
[173] M. Bjorgen, F. Joensen, M. S. Holm, U. Olsbye, K.-P. Lillerud, S. Svelle, *Appl. Catal. A* **2008**, *345*, 43.
[174] C. Mei, P. Wen, Z. Liu, H. Liu, Y. Wang, W. Yang, Z. Xie, W. Hua, Z. Gao, *J. Catal.* **2008**, *258*, 243.
[175] L. Sommer, D. Mores, S. Svelle, M. Stöcker, B. M. Weckhuysen, U. Olsbye, *Microporous Mesoporous Mater.* **2010**, *132*, 384.

[176] M. Moliner, J. Gonzalez, M. Teresa Portilla, T. Willhammar, F. Rey, F. J. Llopis, X. Zou, A. Corma, *J. Am. Chem. Soc.* **2011**, *133*, 9497.
[177] M. Moliner, T. Willhammar, W. Wan, J. Gonzalez, F. Rey, J. L. Jorda, X. Zou, A. Corma, *J. Am. Chem. Soc.* **2012**, *134*, 6473.
[178] T. Willhammar, J. Sun, W. Wan, P. Oleynikov, D. Zhang, X. Zou, M. Moliner, J. Gonzalez, C. Martinez, F. Rey, A. Corma, *Nat. Chem.* **2012**, *4*, 188.
[179] P. Sazama, B. Wichterlova, J. Dedecek, Z. Tvaruzkova, Z. Musilova, L. Palumbo, S. Sklenak, O. Gonsiorova, *Microporous Mesoporous Mater.* **2011**, *143*, 87.
[180] S. Svelle, L. Sommer, K. Barbera, P. N. R. Vennestrom, U. Olsbye, K. P. Lillerud, S. Bordiga, Y.-H. Pan, P. Beato, *Catal. Today* **2011**, *168*, 38.
[181] K. Barbera, F. Bonino, S. Bordiga, T. V. W. Janssens, P. Beato, *J. Catal.* **2011**, *280*, 196.
[182] N. E. R. Zimmermann, S. Jakobtorweihen, E. Beerdsen, B. Smit, F. J. Keil, *J. Phys. Chem. C* **2007**, *111*, 17370.
[183] A. F. Combariza, G. Sastre, A. Corma, *J. Phys. Chem. C* **2011**, *115*, 875.
[184] P. Demontis, G. B. Suffritti, *Microporous Mesoporous Mater.* **2009**, *125*, 160.
[185] V. Kapko, C. Dawson, M. M. J. Treacy, M. F. Thorpe, *Phys. Chem. Chem. Phys.* **2010**, *12*, 8531.
[186] B. Smit, T. L. M. Maesen, *Chem. Rev.* **2008**, *108*, 4125.
[187] P. G. Bolhuis, D. Chandler, C. Dellago, P. L. Geissler, *Annu. Rev. Phys. Chem.* **2002**, *53*, 291.
[188] C. Dellago, P. G. Bolhuis, D. Chandler, *J. Chem. Phys.* **1999**, *110*, 6617.
[189] A. Laio, M. Parrinello, *Proc. Natl. Acad. Sci. USA* **2002**, *99*, 12562.
[190] B. Ensing, A. Laio, M. Parrinello, M. L. Klein, *J. Phys. Chem. B* **2005**, *109*, 6676.
[191] A. Laio, A. Rodriguez-Fortea, F. L. Gervasio, M. Ceccarelli, M. Parrinello, *J. Phys. Chem. B* **2005**, *109*, 6714.
[192] B. Ensing, M. De Vivo, Z. W. Liu, P. Moore, M. L. Klein, *Acc. Chem. Res.* **2006**, *39*, 73.
[193] A. Laio, F. L. Gervasio, *Rep. Prog. Phys.* **2008**, *71*, 126601.
[194] T. Bucko, L. Benco, J. Hafner, J. Angyan, *J. Catal.* **2007**, *250*, 171.
[195] T. Bučko, L. Benco, O. Dubay, C. Dellago, J. Hafner, *J. Chem. Phys.* **2009**, *131*, 214508.
[196] T. Bučko, L. Benco, J. Hafner, J. G. Angyan, *J. Catal.* **2011**, *279*, 220.
[197] L. Benco, T. Bucko, J. Hafner, *J. Catal.* **2011**, *277*, 104.
[198] C. Bai, L. C. Liu, H. Sun, *J. Phys. Chem. C* **2012**, *116*, 7029.
[199] K. Hemelsoet, Q. Qian, T. De Meyer, K. De Wispelaere, B. De Sterck, V. Van Speybroeck, M. Waroquier, B. M. Weckhuysen, *unpublished results*.
[200] S. J. Kim, H.-G. Jang, J. K. Lee, H.-K. Min, S. B. Hong, G. Seo, *Chem. Commun.* **2011**, *47*, 9498.
[201] F. F. Madeira, H. Vezin, N. S. Gnep, P. Magnoux, S. Maury, N. Cadran, *ACS Catal.* **2011**, *1*, 417.
[202] L. Sommer, S. Svelle, K. P. Lillerud, M. Stöcker, U. Olsbye, *J. Phys. Chem. C* **2011**, *115*, 6521.

Received: December 9, 2012
Published online on April 17, 2013